Adsorption of Estrogenic Hormones in Aqueous Solution Using Electrospun Nanofibers From Waste Cigarette Butts: Kinetics, Mechanism, and Reusability

Muhammad Yasir (yasir@utb.cz)
Tomas Bata University in Zlin University Institute: Univerzita Tomase Bati ve Zline Univerzitni institut
https://orcid.org/0000-0001-8999-2779
Tomáš Šopík
Tomas Bata University in Zlin University Institute: Univerzita Tomase Bati ve Zline Univerzitni institut
Rahul Patwa
Tomas Bata University in Zlin University Institute: Univerzita Tomase Bati ve Zline Univerzitni institut
Dušan Kimmer
Tomas Bata University in Zlin University Institute: Univerzita Tomase Bati ve Zline Univerzitni institut
Vladimír Sedlařík
Tomas Bata University in Zlin University Institute: Univerzita Tomase Bati ve Zline Univerzitni institut

Research Article

Keywords: wastewater treatment, estrogens removal, batch adsorption, kinetics, cigarette electrospun nanofibers

Posted Date: September 13th, 2021

DOI: https://doi.org/10.21203/rs.3.rs-837192/v1

Version of Record: A version of this preprint was published at Express Polymer Letters on January 1st, 2022. See the published version at https://doi.org/10.3144/expresspolymlett.2022.46.

Adsorption of estrogenic hormones in aqueous solution using electrospun nanofibers from waste cigarette butts: Kinetics, mechanism, and reusability

Muhammad Yasir*, Tomáš Šopík, Rahul Patwa, Dušan Kimmer, Vladimír Sedlařík*

Centre of Polymer Systems, University Institute, Tomas Bata University in Zlín, Třída Tomáše Bati 5678, 760 01Zlín, Czech Republic

* Corresponding authors: M.Yasir (yasir@utb.cz), V. Sedlařík (sedlarik@utb.cz)

Abstract

This study emphasizes rapid and simultaneous adsorptive removal of estrogenic hormones (EHs): estrone (E1), 17β-estradiol (E2), 17α-ethinylestradiol (EE2), and estriol (E3) from wastewater using recycled waste cigarette electrospun nanofibers (WCENFs). The nanofibers exhibited a small diameter (196±65 nm) and large surface area (18.05 m^2/g), along with a strong affinity towards all EHs by adsorption due to abundant hydrogen bonding interactions. A one-step high-performance liquid chromatography technique was developed to detect each EH present in the solution simultaneously. The adsorption kinetics helps select optimum conditions for the large-scale removal process, so experimental data using pseudo-first-order, pseudo-second-order, intra-particle diffusion, Elovich, and fractional power models were fitted. It was found that E1, E2, and EE2 followed pseudo-second-order kinetics while E3 followed pseudo-first-order kinetic models. The total adsorption capacity on WCENFs was determined to be 2.14 mg/g, whereas the individual adsorption capacities of E1, E2, EE2, and E3 were found to be 0.551, 0.532, 0.687, and 0.369 mg/g, respectively. The percentage efficiency of WCENFs was highest with EE2 ~64.3% and least with E3 ~34.6%. Adsorption-desorption studies revealed that WCENFs could repeatedly be used four times. The reported results indicate a significant potential of WCENFs to be an effective sorbent and portable filter for simultaneous estrogenic hormone removal. WCENFs filter is a suitable alternative to commercial Cellulose acetate filters.

Keywords wastewater treatment, estrogens removal, batch adsorption, kinetics, cigarette electrospun nanofibers

1. Introduction

Reportedly over 5.5 trillion cigarettes are produced all over the globe, and 4.5 trillion waste cigarette butts (CBs) cause about 2 million tons of litter without proper disposal (Torkashvand and Farzadkia 2019; Shen et al. 2020). The CB filter was designed in the mid-twentieth century to capture toxic smoke containing 4000 chemical compounds and hazardous chemicals, with 25% in the tar phase and remaining in the gaseous phase. The contaminants in CBs include heavy metals such as cadmium, nickel, arsenic, chromium, polycyclic aromatic hydrocarbons, formaldehyde, acetaldehydes, hydrogen cyanide, and benzene (Torkashvand and Farzadkia 2019). It is considered one of the most critical waste due to its high dispersion worldwide, causing severe health effects on the lives of humans (Bilge et al. 2019). Cigarette smoking not only causes significant health damage to the smoker but also to the passive smoker, ultimately leading to continuous air pollution. The open disposal of CB in public areas such as bus stops, stations, parks, and gardens pollutes soil and water (Rebischung et al. 2018). It degrades the chemical, physical and biological conditions of nature (Montalvão et al. 2019; Torkashvand and Farzadkia 2019). The available cigarette in the market consists of 95% cellulose acetate (CA) (Benavente et al. 2019); the remaining are paper, polyvinyl alcohol, and tobacco. The CB is approximately 30% of its length and contains monofilament tow of CA combined with some additives and chemicals. The accumulation of traces of tobacco in these CBs and their disposal as wastes is a severe issue and major threat to the ecosystem because CBs are non-degradable. These are flushed away by rain and through drains into rivers, seas, and further into the oceans, which is devastating for marine life (Hemamalini et al. 2019)as the contaminants of CBs are likely to enter the food chain. The collection of CBs requires high cost, and the extraction of toxic chemicals from them requires difficult and much complex methods due to many different kinds of contaminants present (Torkashvand et al. 2020). Thus, it is necessary to identify a new method of recycling CBs to counter this inevitable waste (Alhokbany et al. 2020).

Likewise, synthetic estrogenic hormones (EHs), also called endocrine-disrupting chemicals (EDCs), have an adverse effect on humans and wildlife (McLachlan et al. 2006; Schäfer et al. 2018). Residual of these micropollutants are observed in micro and nanograms in local cleaning reservoirs of wastewater treatment (Schäfer et al. 2018). This issue has aroused deep concerns in the scientific world because these synthetic EHs can interfere with functional groups of

hormones synthesized naturally inside the body by mimicking them (Luo et al. 2015; Montes-Grajales and Olivero-Verbel 2015; Gyllenhammar et al. 2017; Sood et al. 2017; Chen et al. 2018). Thus, the presence of these EHs is a severe threat to both human and aquatic life based on the source of food or drinking water (Han et al. 2010a; Chen et al. 2018).

The most common EHs include estrone (E1), estradiol (E2), ethinylestradiol (EE2), estriol (E3); They harm the reproduction tendency of aquatic species and interrupt natural body hormones function (Han et al. 2010a). Studies have shown an increase in fish femininity, testicles weight loss in quails, and fertility disorder in alligators, which are a few of the many side effects (Nghiem and Schäfer 2002). Furthermore, a decline in male sperm count, high breast and ovarian cancer risks in humans have been reported (Solomon and Schettler 2000). Higher potency of these EHs has been observed at treatment plants downstream (Johnson et al. 2005; Cartinella et al. 2006; Sarmah et al. 2006). EHs in the range of 3.4-41 ng/L have been reported in constructed wetlands of the Czech Republic (Vymazal et al. 2015). Among these estrogens, EE2 is a modern formulated synthetic EH used as an oral contraceptive for treating prostate cancer and menstrual problems in females (Han et al. 2013). Compared with other EHs, EE2 is the most dangerous due to its partial degradation, while its treatment and inadequate removal lead to colossal estrogenicity (Braga et al. 2005). Consequently, when the EE2 hormone gets favorable conditions, it deconjugates the metabolites and becomes active again for interacting with the hormones in the human body (Limpiyakorn et al. 2011). Therefore, EE2 is identified and considered the highest potent in all EDCs (Aris et al. 2014; Adeel et al. 2017; Siegenthaler et al. 2017). Hence, the EHs require proper concurrent disposal and elimination from wastewater.

The conventional wastewater treatment plants cannot properly remove these hormones with low molecular weight and low biodegradability because they are difficult to be detected and quantified at extremely low concentrations (Semião and Schäfer 2010). EHs are widely spread in reservoirs, rivers, and lakes when released with treated effluents (Tijani et al. 2013; Luo et al. 2014). Reportedly, various treatments have been applied, such as ozonation, membrane bioreactors, advanced oxidation, membrane filtration, photocatalytic degradation, and coagulation-flocculation, to counter this issue (Onesios et al. 2009; Pham et al. 2013; Ali et al. 2021). Each technique has some limitations, such as complexity, low efficiency, and by-products

generated during the procedure require further sophisticated purification steps. Nano-filtration and reverse osmosis have also emerged as interesting methods, but the intense energy requirements make them unfeasible for selection (Shannon et al. 2008; Pendergast and Hoek 2011).

Adsorption is one such technique that has been found to address the issue of EH removal with much promise. In addition to the sorption technique, the sorbent material is the most important and dominant factor. Several adsorbents have been reported for EH removal in previous studies, such as granules of activated charcoal (Kumar et al. 2009; Kumar and Mohan 2011), fullerene (Jin et al. 2007; Pan et al. 2008), carbon nanotubes (Kiran Kumar and Venkata Mohan 2012), chitosan, activated carbon, chitin, multi-walled carbon nanotubes, carbon-based adsorbents prepared from industrial waste (Zhang and Zhou 2005; Krupadam et al. 2011), and activated carbon fibers modified with iron hydroxide (Hristovski et al. 2009). All these materials are efficient due to the large surface area they possess, but they require a further separation process from wastewater, which increases the overall cost. Recently, it has been proven that adsorbents such as nanofibers could eradicate the subsequent additional separation step (Wang et al. 2013; Zhao et al. 2017). Thus, the research essentially needs a new high-performance material specifically with an optimum disposal process efficiency.

Recently, nanofibers as sorbents have an emerging interest because of their characteristics features such as light weight, small pore size, and high surface area (Augusto et al. 2013). In the context of recycling materials, electrospinning is one of the methods to fabricate nanofibers. Electrospinning is a versatile technique for generating a continuous nanofiber sheet with a diameter from tens to hundreds of nanometres for sophisticated adsorption and water filtration techniques (Bhardwaj and Kundu 2010; Yang et al. 2010). The filtration efficiency is significantly raised due to small nano diameters, reduced pore size, and the large specific surface area of nanofibers provide a greater contact of the solution with the sorption material (Celebioglu et al. 2014; Yudanova et al. 2016; Gopakumar et al. 2017). The setup requires an applied voltage between the two electrodes to allow electrostatic forces to overcome the polymer's surface tension to eject the polymer solution to form threads onto a rotating drum in the solution bath and solidify non-woven fibers on a collecting electrode covered by non-woven textile to peel off

nanofibers efficiently [7,49,54–56]. Thus, the quality of nanofibers can be improved by producing beadless nanofibers using additives such as polyethylene oxide in a polymer solution (Yudanova et al. 2016).

In literature, electrospun polymers have proven to be an excellent choice for removing heavy metal ions, organic pollutants, and dyes from wastewater (Chigome and Torto 2011; Chigome et al. 2011). Also, for the adsorption of EH, to the best of our knowledge, polyamide (PA) nanofibers have only been reported for the removal of a single E1 or EE2 hormone while polyethersulfone (PES) for E2 removal and polyvinylidene (PVDF) membrane modified with polyvinyl pyrrolidone and titanium dioxide for removal of E1 and E2 (Han et al. 2013; Wang et al. 2016; Schäfer et al. 2018; Niavarani et al. 2021). Additionally, in our previous study, we have reported polyurethane (PU), cellulose acetate (CA), and polyacrylonitrile (PAN) for such estrogenic hormones (unpublished data). Hence, it is necessary to develop and optimize such nanofibers produced from recycling that can reduce litter, behave ideally for removing EH, and require low production cost (Kimmer et al. 2011).

Taking both aspects of recycling and hormone removal by efficient use of an ever-increasing amount of waste CBs will not only keep the environment clean but also will be one of the best possible solutions to overcome the nuisance of EHs. Presently, few studies have been done with CBs in different applications such as asphalt production, biofilm carrier, metal corrosion inhibitors (Torkashvand and Farzadkia 2019), energy storage devices (Alhokbany et al. 2020), insecticides, fired clay brick filler (Hemamalini et al. 2019). However, these CBs can be potentially used to prepare electrospun nanofibers [62], which are efficient in EH removal because they can undergo hydrogen bonding with the hormones due to the presence of oxygen-containing groups in the CA structure (Alhokbany et al. 2020; Filep et al. 2021).

This paper aims to prepare and test possibly WCENFs from the waste CBs with the desired morphology, small fiber diameter, large surface area to the volume ratio, and more sites available for adsorption. We have concentrated on applying nanostructured membrane with high sorption activity for EH removal from wastewater. Such a membrane can be used as a substitute for microfiltration, compared to the commercial microfiltration membranes available in the market

that exhibit higher fluxes (Kimmer et al. 2017). The objective is simultaneous adsorption of various estrogenic hormones in a one-step process from wastewater. Further, to investigate the feasibility of the results using the experimental data to determine adsorption capacity and apply different kinetic models such as pseudo-first-order, pseudo-second-order, intraparticle diffusion, elovich, and fractional power models. These models help to understand the characteristics of adsorption kinetics that are essential for the selection of optimum conditions for the large-scale removal of such EHs. Finally, the study includes establishing the nanofibers' adsorption mechanism and determining the reusability in several adsorption cycles to know their reliable effectiveness. This study shows a comparison of the instant adsorption efficiency of WCENFs against the commercially available CA syringe filter. The newly tested electrospun material must also offer feasibility for large-scale regeneration from CBs.

2. Materials and Methods

2.1. Materials and reagents

The CBs, regardless of brand, were collected over a week from the cigarette waste bins of Centre of Polymer Systems (CPS), Tomas Bata University in Zlin, Czech Republic. Four EHs viz. estrone ≥99% (E1), 17β-estradiol ≥98% (E2), estriol ≥97% (E3), and 17α-ethinylestradiol ≥98% (EE2), were purchased from Sigma-Aldrich Chemie GmbH, Germany. Swinnex filter holders with Luer lock and 25 mm diameter were purchased from Sigma-Aldrich, Germany., acetonitrile (HPLC grade) and ethanol (HPLC grade > 99% pure) were purchased from Honeywell and VWR, Czech Republic, respectively. Furthermore, Sodium tetra-borate decahydrate (borax), citric acid, acetic acid (99%), and formic acid (98%) were purchased from PENTA s.r.o., and N,N-dimethylformamide (DMF >99.5%) from Lach-Ner, s.r.o., Czech Republic. Polyethylene oxide (PEO) from scientific polymer products, Inc, Ontario, USA. Deionized water (18.3 MΩ/cm, pH 7.3) was sourced from a Milli-Q ultra-pure (type1) water purification system, Biopak® Polisher, Merck, USA, and was used throughout the study.

2.2. Nano-fibers fabrication

CBs were washed with distilled water twice to remove unwanted debris and dust and dried in a hot-air oven for 6 h at 80 °C. Further, they were washed with ethanol and kept at 40 °C for 4 h. A total of 8 wt.% of CBs were dissolved in a binary solution of acetic acid and formic acid in a 2:1

ratio to make a total solution of 400 g. Then, 3 wt.% of PEO of the amount of the CBs was added for stability of the mixture to improve the structural properties of nanofibers. Finally, the mixture was stirred for 5 h at 400 rpm in a mechanical stirrer (Heidolph, RZR 2041). Electrical conductivity was adjusted to about 88.1 µS/cm by using a solution of borax and citric acid (BC) in 1:3 prior to electrospinning; which was prepared by dissolved 35 wt.% of BC in DMF solution and stirring for 5 h at 400 rpm on a magnetic stirrer and viscosity of the solution during the preparation was kept at 0.95 Pa.s.

The electrospinning process was performed by nano spider technology using the NS Lab 200S equipment (Elmarco, Czech Republic) to produce WCENFs on a polypropylene spun-bond non-woven sheet with a width of 40 cm. The applied supply was 75 kV, solution coming out of the bath to be sprayed from cord strings was set at 0.34 mL/min the distance between the electrodes was 18 cm, the rotational speed of collecting fiber sheet fabric was 10 cm/min, the temperature was 27 ± 1 °C with the relative air humidity < 35%. The solution properties were optimized before the electrospinning process, and the properties of the WCENFs are shown in Table 1.

Table 1

Representative properties of the solution prior to electrospinning and of WCENFs

Sample	Concentration (%)	Density (g/cm^3)	Intrinsic Viscosity (Pa.s)	Electrical conductivity (µS/cm)	Average area mass (g/m^2)
Cigarette	8	1.32	0.95	88.1	0.865

The table above shows the optimized properties of the polymer solution prepared for electrospinning and the average area mass of produced electrospun nanofibers. The aim of optimizing these parameters was to produce defect-free and beadless nanofibrous mats from waste CBs.

2.3. Characterization

Morphological analysis was carried out using Nova 450 scanning electron microscope (SEM) (FEI, Thermo Fisher Scientific, USA) at 5-10 kV applied potential using a through-the-lens detector (TLD). It was done to observe the fiber surface morphology, the diameter of fibers, and

the defects in the structures such as beads. The software ImageJ version 1.52a was used to determine the average fiber diameter of samples.

X-ray diffractogram (XRD) of WCENFs was recorded using Miniflex^{TM} 600 X-ray diffractometer (Rigaku, Japan), having CoK_{β} (λ=1.79 Å) as a source. The angle 2θ was in the range from 5-90° with operating current, step size, step time, and operational voltage set to 15 mA, 0.02°, 10°/s, and 40 kV, respectively. The diffractograms obtained using Co source were converted to Cu using PowerDLL software converter 2.93 to compare data in the prior art.

To determine the functional groups present in WCENFs used for the adsorption of EHs, Nicolet 320 Fourier transformed infrared spectroscopy (FTIR) (ThermoScientific, USA) equipped with Ge crystal was used. The attenuated total reflectance (ATR) spectra were recorded from 400-4000 cm^{-1}at ambient temperature with a scan rate of 16 and a resolution of 4 cm^{-1}.

The surface area analysis of WCENFs was made utilizing the Brunauer-Emmett-Teller (BET) high precision surface area and pore size analyzer BELSORP-mini II (BEL Japan, Inc., Japan) to determine the specific surface area. The substrate's outgassing was done at 100 °C for 12 h under vacuum before starting measurement. Air permeability and pore size distribution of nanostructure were assessed by flow porometer according to ASTM F316-03 (2011). Galpor (Porometer NV, Belgium) was used as a wetting liquid.

To determine the contact angle of the electrospun nanofibers, they were made more compact for accurate measurement. First, the WCENFs on polypropylene (PP) substrate were placed upside-down on the Polyethylene terephthalate (PET) sheet and subjected to thermal press for 10 seconds at a temperature of 120 °C, and then, PP was detached. Next, the WCENFS on PET were covered with a glossy sheet for a thermal press again with the same conditions to acquire a smooth and more compact surface. This step was done so that liquid could stay on the surface for angle measurement; otherwise, the surface would not hold the drop in the case of WCENFs on PP, and it would instantly settle down and penetrate through the structure. Finally, the contact angle of electrospun nanofibers was measured using the sessile drop technique on a goniometer (Surface Energy Evaluation System (SEE System), Advex Instruments, Brno, Czech Republic) at

ambient temperature. A 5 µL pipette was used to drop liquid on the sample surface (10 × 10 mm^2), the drop shape was observed using CCD camera, and the angle was measured instantly. Glycerol and Milli Q water were used as the probe liquids to determine the hydrophilicity and surface free energy (SFE) calculation because of their various dispersive and polar components of surface tension along with their low vapor pressure value (Szewczyk et al. 2018). The samples were analyzed in triplicates, and average values were reported. The SFE for the WCENFs was determined using the Owens, Wendt, Rabel, and Kaelble (OWRK) method that is governed using Eq. (1) as follows (Patwa et al. 2020):

$$\frac{1}{2}(1 + cos\theta)\frac{\gamma_L}{\sqrt{\gamma_L^D}} = \sqrt{\gamma_S^P}\sqrt{\frac{\gamma_L^P}{\gamma_L^D}} + \sqrt{\gamma_S^D} \quad (1)$$

where, γ_L is the surface tension, γ_L^P and γ_L^D are polar and dispersed fractional components of the liquid, respectively (values obtained from literature) and γ_S is the SFE of the solid.

The thermal stability of the nanofibers was determined using a TGA Q500 thermogravimetric analyzer (TA Instruments, USA). Sample (~19.0±0.5 mg) depending on density was heated in alumina crucible from 25 to 700 °C at a ramp of 15 °Cmin^{-1} under N_2 flow of 100 m$Lmin^{-1}$. To determine the thermal behavior and properties of WCENFs, they were subjected to differential scanning calorimeter (DSC) star®System (Mettler Toledo, Switzerland). The sample (5.0±0.5 mg) was sealed in an aluminum pan under a nitrogen flow of 50 m$Lmin^{-1}$ and heated from 25 to 320 °C at a ramp of 10 °Cmin^{-1}.

Gel permeation chromatography (GPC) used a Waters HPLC system equipped with a Waters model e2695 and a Waters model 2414 differential refractometer to determine the mass average molar mass (*Mw*), number average molar mass (Mn), and polydispersity index (*PDI= Mw/Mn*) of the tested WCENFs samples from peaks corresponding to the polymer fraction using the absolute calibration method (Waters Corporation, Milford, USA). The WCENFs were dissolved in Tetrahydrofuran (THF) (2–3 mg/mL), stabilized with Butylated hydroxytoluene (BHT) (240 mg/L), and filtered through a 0.45 µm syringe filter. The following procedure was used to separate the samples on a series of gel-mixed bed columns (Polymer Laboratories Ltd, Shropshire, UK): 1 × PLgel-Mixed-A bed column (300 × 7.5 mm, 20 µm), 1 × PLgel-Mixed-B bed column (300 × 7.5 mm, 10 µm), and 1 × PLgel-Mixed-D bed column (300 7.5 mm, 5 µm); at

40 °C, the mobile phase contained THF stabilized with BHT (240 mg/L). The mobile phase flow rate was set to 1.0 mL min^{-1}, and the injection volume was 100 µL. All data processing was carried out using Empower 3 software. (supplementary data, Table S1)

To see the strength of nanofibers, the tensile test of PP neat and PP with WCENFs was performed and compared because pure WCENFs were very fragile, it was difficult to peel them from PP to prepare a dumbbell shape and perform a tensile test. Further to test the WCENFs filter in the last section, PET was used as a support for pure WCENFs. Therefore, the tensile tests of PP, PP/WCENFs), and PET/WCENFs were carried out on an M350-5CT tensile testing machine (Testometric, UK) supplied with a load cell of 10 kgf. For all measurements, a crosshead pull speed of 10 mm/min and a gauge length of 20 mm was used. A unique die was used to cut specimens in the shape of dumbbells (Type 3, ISO 37:2005). Young's elastic modulus (MPa), ultimate tensile strength (N/mm), percentage elongation (%), and other mechanical properties were obtained. Measurements were conducted in triplicates, and mean values with standard deviation were reported.

2.4. High-Performance Liquid Chromatography (HPLC) analytical method

An HPLC DionexUltiMate 3000 Series was used to analyze EHs (E1, E2, EE2, E3) calibration standards and samples (Thermo Fisher Scientific, Germany). At 30 °C, the separation was carried out on a Kinetex 2.6 µm C18 100 A (150x4.6mm; Phenomenex, USA) reversed-phase column with a pre-column security guard ULTRA, UHPLC C18 (Phenomenex, USA). A mobile phase of HPLC grade acetonitrile and water (45:55, vol/vol) was utilized at a flow rate of 0.8 mL/min for a total isocratic run of 12 min. A volume of 20 µL was injected into the column, and the sampler chamber was set at 5 °C. At wavelengths of 200 and 205 nm, eluates were recorded. The EH concentration was determined using the 200 nm test results (supplementary data, Fig. S1). The external calibration method for quantification of concentration was performed using the Chromeleon version 7.2 software (Thermo Fisher Scientific, USA) (YASIR et al. 2020).

2.5. Solution preparation and sampling

A solution containing all EHs was prepared by adding 1 mg of each EH in 5 L of water, kept under magnetic stirring at 800 rpm for 24 h, making an overall concentration of 0.8 mg/L solution and individual concentration of 0.2 mg/L. Samples in a concentration of 0.2, 0.15, 0.1,

0.05, 0.03, 0.02, 0.005 mg/L were collected using a micropipette (HTL Lab Solution, Poland) in 1.5 mL screw neck vials (VWR, Czech Republic) after passing through glass microfiber (GMF) filter (Whatman, Czech Republic) with pore size 0.45 µm and 25 mm in diameter before HPLC. A calibration curve was obtained using mean concentrations from triplicate values. The calibration vial with a concentration of 0.005 mg/L was used to identify each hormone's detection limit. The limit was set at 0.5, 1.0, 2.0, and 5.0 µg/L for E3, E2, EE2, and E1, respectively.

2.6. Batch adsorption tests of WCENFs

The experimental kinetics were carried out to determine the adsorption rate. Tests for WCENFs were performed in triplicates using 100 mL of EH solution taken from stock with a total concentration of 0.8 mg/L, and 20 mg of WCENFs were placed in each flask. The flasks were continuously stirred at 250 rpm using an orbital incubator shaker (GFL 3005, MERCI s.r.o., Germany). To determine the remaining concentration of EHs present in the solution, samples were drawn at fixed intervals of time each after 5 min, 15 min, 30 min, 60 min, and after each hour until a plateau was reached. At each time point, 4 mL samples were drawn using a 20 mL syringe and collected in vials after passing through a 0.45 µm GMF filter. The first 2 mL filtrate was discarded by passing from a syringe through a GMF filter to eliminate any negligible adsorption within the filter and rinse out any remaining liquid from the previous reading while sampling to ensure accuracy and precision. Proper care was taken to ensure that neither nanofiber was removed nor destroyed during the sampling and was replaced by 4 mL of ultrapure water to maintain the total sample volume. A flask containing a solution without nanofibers labeled as control was placed in the experiment as a starting reference concentration. It must be noted that adsorption on the glass surface was negligible throughout the long-term testing. Then, the results of triplicated experimental values were obtained to calculate average concentration values and standard deviations that were recorded and reported. Finally, the percentage of adsorption of each EH on WCENFs was calculated with reference to the control. The solution was maintained neutral at a pH of 7.3. The percentage removal of each EH at a given time (t) was measured using the expression shown in Eq. (2) as follows (Al-Khateeb et al. 2014a; Qi et al. 2014):

$$Removal\ (\%) = \frac{C_i - C_t}{C_i} \times 100 \quad (2)$$

where C_i is the initial concentration (mg/L) and C_t is the concentration of solution at time t (mg/L).

Also, Equilibrium adsorption capacity (q_e) and adsorption capacity (q_t) at time t can be calculated by the following expressions shown in Eq. (3) and Eq. (4) (Zhao et al. 2017; Abdel-Gawad and Abdel-Aziz 2019):

$$q_e = v \times \frac{C_i - C_e}{m} \quad (3)$$

$$q_t = v \times \frac{C_i - C_t}{m} \quad (4)$$

where m is the mass of adsorbent in grams and v is the volume of solution in liters.

2.7. Desorption and reusability of material

To determine the reversibility of WCENFs sorption, the nanofibers in triplicates were taken out from the EH solution and washed thoroughly with distilled and deionized water followed by immersion in 50 mL of water and shaken for 20 min at 250 rpm. This step would just clean the surface of nanofibers and nominally remove some physically adsorbed hormones, but it would not significantly reduce EH concentration on nanofibers due to chemical bonding (Schäfer et al. 2018). The nanofibers were then placed in the oven at 30 °C for 6 h to remove the excess moisture, followed by air drying without any effect on nanofibers. This step was repeated thrice followed by immersing in 40 ml pure anhydrous ethanol, given that all estrogenic hormones have a very high solubility in ethanol based on their high partitioning coefficient (Log- $K_{o/w}$ = 3.13, 4.01, 2.45, and 3.90 for E1, E2, E3, and EE2, respectively). Then, a strong partition effect was expected to occur in combination with a competing hydroxyl group present in ethanol that could destabilize the EH-nanofiber hydrogen bonds and attract the adsorbed hydrophobic hormones in the ethanol solution (Han et al. 2010a, 2012). Next, the solution system was gently stirred for 30 min at 175 rpm for complete elution of EHs from the nanofibers; after that, air-dried at room temperature and placed in a desiccator until used for the next adsorption cycle. The procedure was repeated for several cycles until very low adsorption was experienced.

2.8 Fabrication of WCENFs syringe filter

To perform the syringe filter test, the WCENFs compressed on the PET sheet were used instead of WCENFs on the PP sheet because PP can itself adsorb hormones as reported to be 96.3% of

E1 with 0.2 µm membrane filter (Han et al. 2010b). This can deteriorate the actual results of WCENFs while not in the case of PET, as they do not contribute to any adsorption. Furthermore, PET is stiffer, providing better strength and holding high pressures during the filtration process (Ma et al. 2012). Therefore, firstly adsorption of EHs was tested on a pure PET mat to see any influence of adsorption. A batch adsorption test was conducted in the same manner as for WCENFs, and no adsorption of any EH was observed on PET. The HPLC chromatograms of solution before and after adsorption perfectly overlap, and there was no decrease in hormone concentration (supplementary data, Fig. S2). Then, WCENFs compressed on a PET sheet were cut into a 25 mm circular disc in triplicates and placed in the swinnex filter holders.

3. Results and discussion

3.1. Characterization of adsorbent

SEM imaging was carried out for morphological analysis of the electrospun nanofibers.

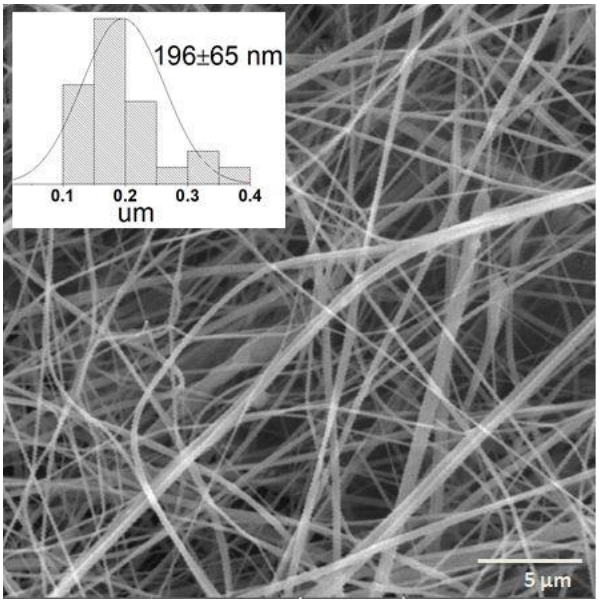

Fig. 1 SEM micrograph and (inset) size distribution for WCENFs

Fig. 1 illustrates that uniform nanofibers were produced with minimum possible beads and a relatively narrow fiber diameter distribution of 196 ± 65 nm. Such low average diameter is attributed to properties mentioned in Table 1: lower intrinsic viscosity, low polymer concentration in the solution, and high electrical conductivity prior to electrospinning, which has led to the development of a high surface area of WCENFs. To further understand the physicochemical properties of the structure, XRD results (supplementary data, Fig. S3) revealed

a broad single peak near 2θ=20°, which denotes that WCENFs contain CA and are semi-amorphous by nature (Taha et al. 2012). The mean diameter of pores in nanostructure was 1.4 µm, and the maximum pore diameter was 2.2 µm. The permeability of nanostructure for the dry air was 247 $L.min^{-1}.bar^{-1}.cm^{-2}$ (supplementary data, Fig. S4 and S5). Also, the results from the TGA thermograph (supplementary data, Fig. S6) showed that no material degradation was observed up to 110 °C, the degradation temperature is found to be 355.7 °C (Arroyo et al. 2020). DSC thermogram revealed that the glass transition temperature (*Tg*) of WCENFs is well above standard room operating temperatures and given that the material melts around 215 °C, which indicates that the material was thermally stable; therefore, these nanofibers will not be subjected to any softening and deformation at room temperature during the whole adsorption studies (supplementary data, Fig. S7) (Benavente et al. 2019; Alhokbany et al. 2020).

Using ImageJ analysis software, the average diameter was obtained for the nanofibers observed through SEM. Considering the fiber as a single continuous cylinder, the length per unit mass (*l/m*) and surface area (*A*) of the fiber can be calculated using the expressions given in Eq. (5), (6), and (7) below (Schäfer et al. 2018).

$$V = \frac{m}{\rho} = \frac{\pi d^2 l}{4} \tag{5}$$

By rearranging this expression, we get:

$$\frac{l}{m} = \frac{4}{\rho \pi d^2} \tag{6}$$

where *V* is the volume (m^3), *m* is the mass (mg), *d* is the diameter of nanofiber (m), and ρ is the density of material (1.32 g/cm^3).

Since l >> d; therefore, individual cross-sectional area (*A*) of the end corners of the fibers can be neglected, and the total surface area per unit mass can be expressed as:

$$\frac{A}{m} = \frac{d\pi l}{m} = \frac{4}{\rho d} \tag{7}$$

The calculated diameters from the SEM images, calculated fiber length, surface area using the above formulas, the surface area measured by BET, and porosity by porometry are shown in Table 2.

Table 2

Characteristics values of WCENFs calculated using SEM micrographs, BET, and porometry

BET before adsorption		BET after adsorption		Porometry		Nanofiber analysis from SEM	
BET surface area (m^2/g)	18.05	BET surface area after adsorption (m^2/g)	3.61	Mean pore size porometry (µm)	1.4	Average fiber diameter SEM (nm)	196 ± 65
BET Mean pore diameter (nm)	13.49	BET Mean pore diameter after adsorption (nm)	17.19	Maximum pore size porometry (µm)	2.2	Fiber length per unit mass calculated (m/mg)	25105
BET Total pore volume (cm^3/g)	0.061	BET Total pore volume after adsorption (cm^3/g)	0.016	Air permeability porometry ($l/cm^2.min.bar$)	247	Calculated surface area (m^2/g)	15.5

The geometrically determined surface area based on SEM compared to that by BET analysis is well in compliance. The BET surface area is well comparable to the literature values in the range of 9-51 m^2/g and 167-2737 nm of the average fiber diameter (Schäfer et al. 2018). The calculated surface area from the average fiber diameter (196 ± 65 nm) considered as cylindrical shape calculated from SEM is 15.5 m^2/g. The actual surface area measured from BET is 18.05 m^2/g which is slightly higher. The plausible reason for lower surface area value based on geometry compared with BET value could be due to much lower density than the bulk polymer density because of pore formation and other effects during electrospinning. The presence of pores is also confirmed by porometry. Furthermore, the estimated surface area is based on the assumption that the fibers have a smooth surface. In reality, solvent evaporation during electrospinning has resulted in a rough surface seen from the SEM micrograph (see Fig. 1) and therefore increased surface area. We can also see that the surface area of nanofiber decreased after adsorption from 18.05 to 3.61 m^2/g. However, the mean pore diameter increased from 13.49 to 17.19 nm due to the wear-off of material during several cycles. Still, a reduced total pore volume was observed

from 0.061 to 0.016 cm^3/g, which justifies the adsorption and entrapment of hormones in the nanofibers during interaction in the batch adsorption study.

Fig. 2 shows the IR spectra of the WCENFs.

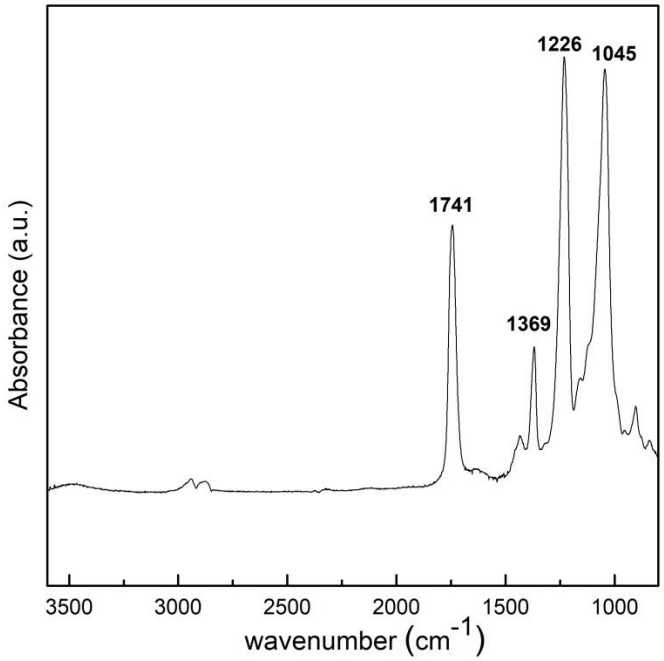

Fig. 2 Attenuated total reflectance (ATR) mode FTIR spectra of WCENFs

The ATR-FTIR characterization of WCENFs was performed to observe the functional groups present. The broadband at 3480 cm^{-1} indicates OH group presence in nanofibers. The characteristic bands at 2941 and 2877 cm^{-1} show symmetric and asymmetric C-H stretching, respectively, the peak at 1741 cm^{-1} implies C=O bond stretching of the carbonyl group. The absorbance peak at 1369 cm^{-1} is for C-CH_3, the peak at 1226 cm^{-1} is for (C-O-C) anti-symmetric stretching bond of the ester group, and finally, a vibration peak at 1045 cm^{-1} can be seen for the C-O bond (Nasir et al. 2017). Hence, the FTIR spectra measured on nanofibers are strongly compliant with the original spectra of cellulose acetate present in the IR spectra bank (Benavente et al. 2019).

The contact angle was measured to determine the hydrophilicity of the nanofibers. WCENFs mainly contain CA, which has polar hydroxyl groups. Thus, CA is hydrophilic by nature (Mikaeili and Gouma 2018). We observed both the liquids penetrated the pure WCENFs completely. Therefore, WCENFs were compressed on a PET sheet, and it exhibited low contact

angle values because we observed water percolation into fiber networks. The contact angles and SFE values are shown in the following Table 3.

Table 3

Contact angle and surface free energy (SFE) values for WCENFs

Contact angle		Surface free energy (γ_s), mN/m	fractions	
Water	Glycerol		Polar (γ_s^P)	disperse (γ_s^D)
14.6±3.3	87.3±0.8	354.4	264.0	90.4
				
Water (contact angle)		Glycerol (contact angle)		

It is generally agreed that a hydrophilic surface shows a low water contact angle ($\theta<90°$). The electrospun nanofibers have a higher contact angle compared to the films of the same polymer (Szewczyk et al. 2018). It is reported that the surface roughness, average fiber diameter, and concentration of the polymer in the solution before electrospinning also have a direct influence on the wetting properties (Mikaeili and Gouma 2018; Szewczyk et al. 2018). They reported spin-coated CA film has a contact angle of 63.67° and that the maximum contact angle with a rough surface can not exceed approximately 109° for 9% w/v of CA. The investigated material in the current study possesses contact angles lower than 90°, a low wetting angle, and a high surface free energy value, which shows that WCENFs are hydrophilic. Another study explained that doping graphene oxide (GO) in Polylactic acid (PLA) could reduce the contact angle of PLA by 9° to improve the hydrophilicity of the surface for enhancing hydrogen bonding interactions between water and groups containing oxygen in GO (Pinto et al. 2013). Therefore, the hydrophilic nature of WCENFs provides feasibility to the nanofibers to interact with EHs in water and support the adsorption process.

To see the mechanical properties of WCENFs, the stress vs. strain graph below explains Young's modulus, ultimate tensile strength, maximum elongation before fracture, and stress at breakage.

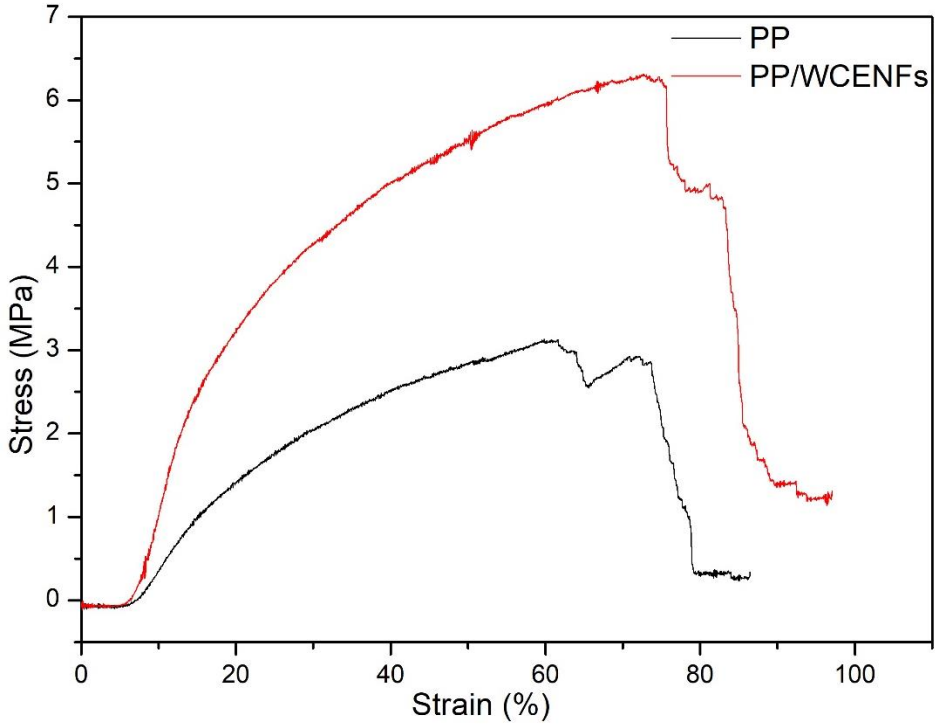

Fig. 3 Stress vs. strain curves for PP and PP/WCENFs

Fig. 3 demonstrates the stress vs. strain curve of PP and PP with WCENFs up to the breaking point. It can be seen that Young's modulus has increased from 8.9 to 28.8 MPa, which is evident from the steep slope in the graph, and the ultimate tensile strength has improved to almost 122% (3.1 to 6.9 N/mm^2). Similarly, a slight increase in stress at breakage from 0.4 to 1.4 MPa and the total elongation increases from 19.3 to 19.9 mm, showing that WCENFs are more flexible than the PP sheet. The values are reported below in Table 4.

Table 4

Summary of mechanical properties of the PP and PP/WCENFs

Materials	Young's Modulus, E (Mpa)	Ultimate Tensile Strength, σ (N/mm^2)	Elongation at break, ε (mm)	Stress at Break (MPa)
PP	8.9±4.3	3.1±1.0	19.3±5.1	0.4±0.2
PP/WCENFs	28.8±2.4	6.9±1.2	19.9±0.7	1.4±0.2

Similarly, the mechanical properties were observed for fabricated PET/WCENFs filter, and an improvement in strength and Young's modulus was reported to be 7.5 N/mm^2 and 109 MPa, respectively. The results from mechanical testing are reported in the supporting data (supplementary data, Fig. S8 and Table S2).

3.2. Batch adsorption study of EHs on WCENFs

The study of four EHs (E1, E2, EE2, E3) was conducted with a total concentration of 0.8 mg/L and 20 mg of WCENFs. Fig. 4a below shows the batch adsorption study of each hormone on WCENFs for a period of time when no significant adsorption was observed, and the material reached almost saturation.

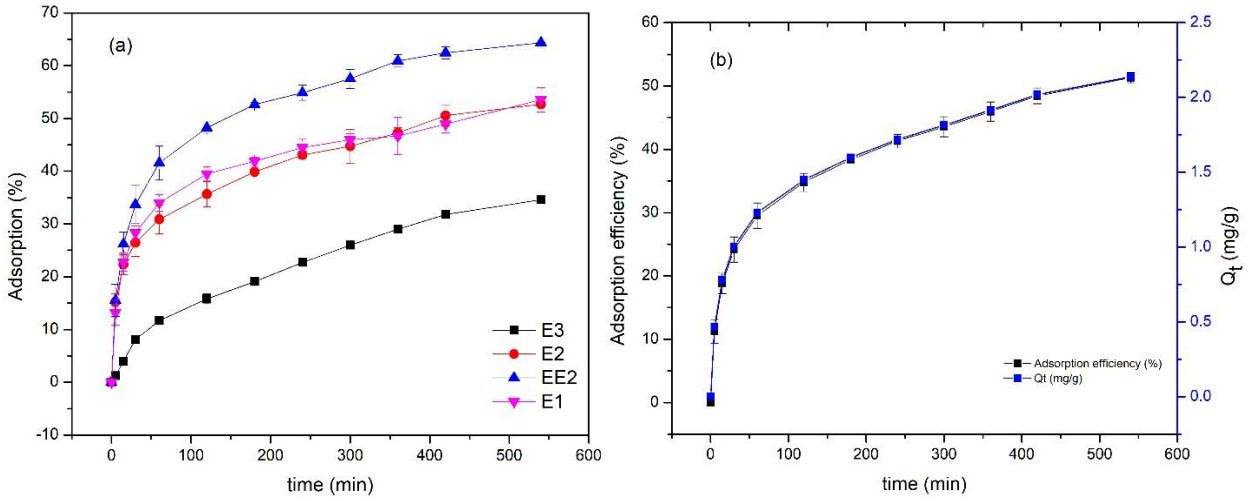

Fig. 4 (a) Batch adsorption study of each EH on WCENFs from a combined solution, (b) Cumulative removal efficiency as a function of time of EHs (E1, E2, EE2, E3) together on WCENFs on the primary y-axis, and the total adsorption capacity of WCENFs as a function of time on the secondary y-axis

Fig. 4a depicts WCENFs adsorption behavior with each hormone, and as can be seen, the ascending order of adsorption of EHs is as E3<E2<E1<EE2 with removal efficiencies of 34.6%, 52.7%, 53.6%, and 64.3%, respectively. WCENFs show the best sorption of EE2 and the worst sorption of E3 hormone. It could also be concluded that WCENFs can readily adsorb EE2, E2, E1, and adsorption of E3 being gradual. The low % removal of E3 could be attributed to its low log K_{ow} value; 2.45, compared with E1, E2, and EE2; 3.43, 3.94, and 4.15, respectively. The adsorption of these estrogens is directly dependent on their hydrophobic nature, which is specified by the higher value of K_{ow} (Al-Khateeb et al. 2014b). Furthermore, E3 follows a

different kinetic trend than the other EHs because the adsorption is gradual throughout the experiment. While for other EHs, most of the adsorption occurs within 30 min from the start. WCENFs have similar adsorption behavior for all EHs compared to the commercial CA, which also follows adsorption efficiency in decreasing order of EE2>E1>E2>E3 (unpublished data). However, the removal efficiencies of EHs with WCENFs are more significant than commercial CA electrospun nanofibers. Hence, it can be concluded that electrospun WCENFs can be sufficiently responsible for the adsorption of each EH simultaneously.

Fig. 4b above shows the percentage of total cumulative adsorption of EHs on WCENFs and the total adsorption capacity of WCENFs in a given time. The results show that the total equilibrium removal efficiency lies at 51.3%. It is evident from the graph that WCENFs had a high adsorption tendency and fast adsorption rates reaching close to half of their efficiency within the first 30 min, as represented by the steep initial slope of the graph corresponding to the removal efficiency mark of about 25%. However, the trend of gradient changes from steep to steady after almost 60 min of continuous adsorption experiment till the end.

The total adsorption capacity (Q_t) as a function of time is also demonstrated in the same Fig. 4b with a secondary y-axis. The results indicate that the cumulative of four EHs' adsorption capacity increases similarly for WCENFs until equilibrium was established between the adsorbates and adsorbent. The time to reach equilibrium depends on the concentration of adsorbate and the amount of adsorbent (Vazquez-Velez et al. 2020). Both factors were kept constant to compare the capacities with the literature. However, it is still necessary to increase the amount of adsorbent to enhance the removal efficiency with a lesser time. The equilibrium adsorption capacity of WCENFs was found to be 2.14 mg/g, and adsorption capacities of E1, E2, EE2, and E3 were found to be 0.551, 0.532, 0.687, and 0.369 mg/g, respectively. Compared to the literature, Yasir *et al*. reported the equilibrium adsorption capacity of commercial CA to be 2.095 mg/g and individual adsorption capacities of E1, E2, EE2, and E3 to be 0.506, 0.532, 0.668, and 0.389 mg/g, respectively. However, the highest equilibrium adsorption capacity was observed for PU Elastollan of 2.51 mg/g and the lowest for PAN of 1.51 mg/g (unpublished data). Furthermore, they also reported the adsorption capacities for E1, E2, EE2, and E3 to be 0.801, 0.592, 0.736, and 0.382 mg/g for PU Elastollan and 0.396, 0.370, 0.343, and 0.397 mg/g for

PAN, respectively. Therefore, the results of WCENFs are well in the range and strongly comply with the literature values.

Furthermore, EE2 is found to have a strong affinity for adsorption as a result; highest adsorption capacity compared to the other three EHs for all the other polymers mentioned in the literature. The adsorption capacities for MWCNTs in literature were found to be 0.423 mg/g, 0.472 mg/g, and 0.472 mg/g, and for the activated sludge were 2533.34 ng/g, 2020.78 ng/g, and 2234.09 ng/g for E1, E2, and EE2, respectively, which are lower values compared to the current research. Furthermore, the value for removing E1 was 62 ng/g when a hydrophobic hollow fiber membrane was used (Al-Khateeb et al. 2014a). Thus, comparing the present study's adsorption capacity with the previous research works shows the suitability of WCENFs as a potential adsorbent for removing these EHs comparing the other solid particles and membrane adsorbents. Hence, it is evident that WCENFs have a pretty high adsorption capacity and are a useful polymeric material for reusing it for these EHs' adsorption.

3.3. Adsorption kinetics

The removal of EHs on WCENFs by adsorption increased with time, obtaining a maximum value for reaching equilibrium. The adsorption rate is fast initially until 30 min and gradually decreases as the contact time increases to an assuming plateau at 540 min. The results obtained from the experiment were used for studying the factors affecting the adsorption process and the rate-limiting step in this process, such as transfer of mass and type of chemical interaction processes. In addition, kinetics information helps in selecting optimum conditions for full-scale removal of the EH process. However, it is often difficult to determine the kinetic parameters and explain the mechanisms involved in the complex heterogeneous systems because the surface effects can superimpose on the chemical effects. Therefore, to further understand the adsorption behaviors and mechanism, parameters from five models; Pseudo-first-order, Pseudo-second-order, and weber-Morris intra-particle/membrane diffusion, Elovich and fractional power model equations are used to test the experimental data to examine the adsorption kinetics of four EHs uptaken by WCENFs. These models are used best to describe the liquid/solid systems. The pseudo-first-order by Lagergren is a widely used and most common model for any adsorption study of different solutes in an aqueous solution. It explains that the rate of sorption of EHs on

570 the surface of the nanofibers is proportional to the number of hormones adsorbed from the
571 solution phase, and it can be expressed by Eq. (8) as (Luo et al. 2017; He et al. 2018):

572 $$q_t = q_e(1 - \exp(-k_1 t)) \quad (8)$$

573 Where q_t is the amount of hormone adsorbed per unit mass at time t (mg/g), q_e is the amount of
574 hormone adsorbed per unit mass at equilibrium (mg/g), and k_1 is the first-order rate constant
575 (L/min).
576
577 The pseudo-second-order equation is related to the solid phase adsorption capacity and can
578 usually predict kinetics behavior over a long adsorption range (Günay et al. 2007). In this model,
579 surface adsorption is the rate-determining step involving chemisorption because of
580 physicochemical interactions between the solid and liquid phases (Ersali et al. 2013). Therefore,
581 the linear form of the Eq. (9) can be expressed as (Esmaeeli et al. 2017; Ye et al. 2021):

582 $$\frac{t}{q_t} = \frac{1}{k_2 {q_e}^2} + \frac{t}{qe} \quad (9)$$

583 Where k_2 is the reaction rate constant (g/(mg min)).
584
585 Usually, the adsorption process occurs in consecutive steps; these include movement of the
586 adsorbate from the solution bulk to the surface of the adsorbent and then diffusion through the
587 boundary layer to the outer surface of the adsorbent. It is followed by the adsorption on an
588 available active site on the adsorbent's surface and, at last, intra-particle diffusion through pores.
589 The Weber-Morris intra-particle/membrane diffusion model is diffusion-controlled; the
590 adsorption rate directly depends on the speed at which an adsorbate can diffuse towards the
591 provided adsorbent. Therefore, this model is described using the Eq. (10) as following (Tian et
592 al. 2011):

593 $$q_t = kt^{\left(\frac{1}{2}\right)} + I \quad (10)$$

594 Where k is the reaction rate constant (mg/g $h^{1/2}$), and I is the y-intercept constant (mg/g), gives
595 the information about the boundary layer thickness.
596 For the validity of this model, it is essential to note that the linear converging line for each EH
597 must pass through the origin for intra-particle diffusion to be the rate-determining step.
598

In reactions where chemisorption is a dominant mechanism such that on the surface of the adsorbent, adsorbate is deposited without desorption of products, the rate of adsorption decreases with time as the reaction proceeds, and it is due to the surface coverage. In such reactions, the elovich model is suitable for explaining the chemisorption process by expressing the following linear Eq. (11) (Günay et al. 2007; Al-Khateeb et al. 2014a):

$$q_t = \beta \ln(\alpha\beta) + \beta lnt \quad (11)$$

Where α and β are the coefficients such that α represent the initial adsorption rate (g/mg min)) and β represents the desorption coefficient (mg/(g min)). These coefficients can be calculated from the slope and y-intercept of the plot given in Fig. 5d.

The fractional power model is the more advanced form of the Freundlich equation, and the linear form is expressed in Eq. (12) (Ho and McKay 2002).

$$lnq_t = lna + blnt \quad (12)$$

Where a and b are the coefficients in the expression and given that b < 1, the product of a and b is given as the specific adsorption rate at 1 min after the start of the experiment.

The adsorption kinetic plots for the adsorption of four EHs on WCENFs are shown in Fig. 5, and the obtained kinetic parameters from the models mentioned above are presented in Table 5.

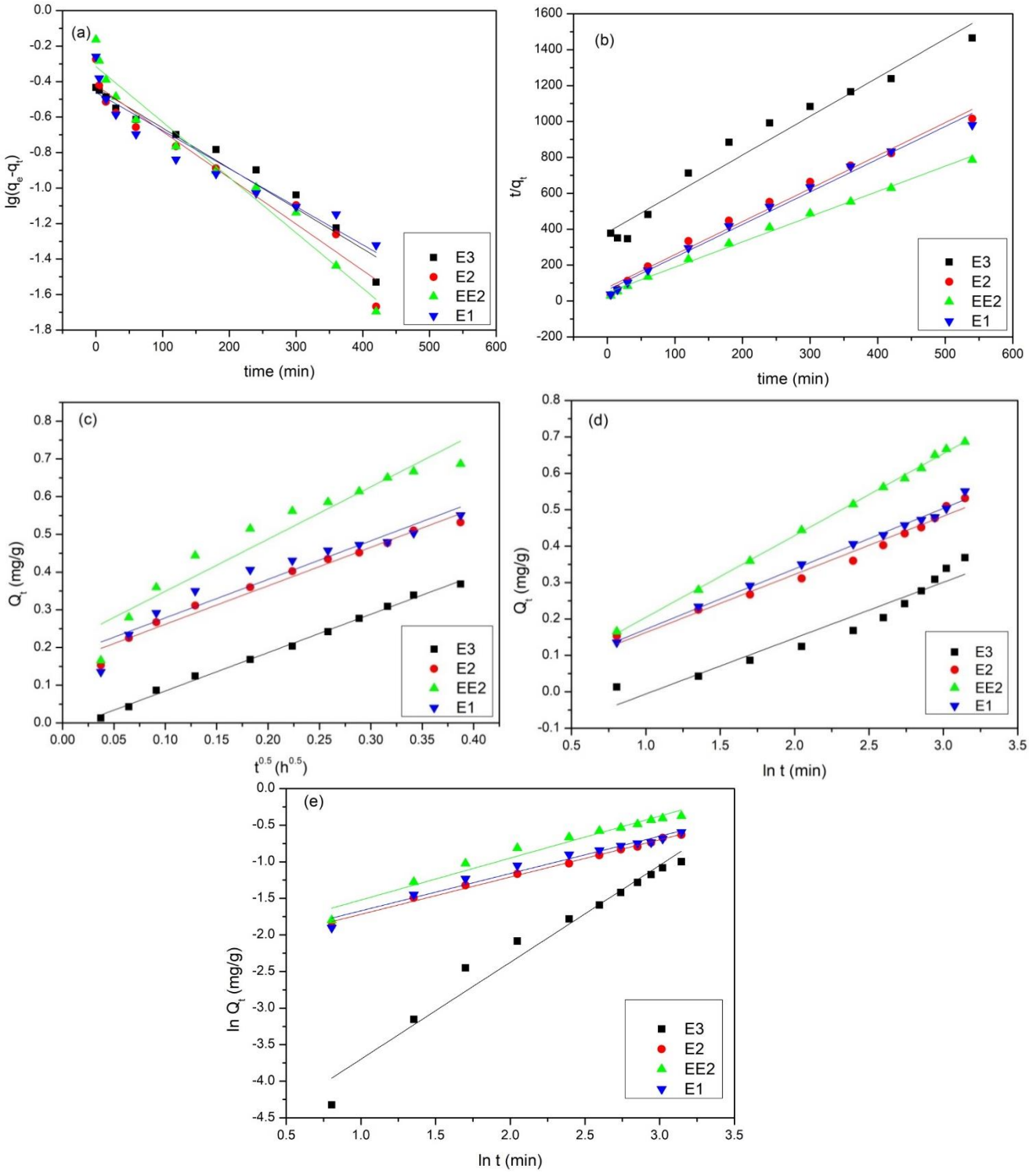

Fig. 5 Adsorption kinetics plots of four EHs (E1, E2, EE2, E3) on WCENFs, (a) Pseudo-first-order, (b) Pseudo-second-order, (c) Weber-Morris interparticle diffusion model, (d) Elovich model, and (e) Fractional power model

629 The results were examined to obtain adsorption kinetics fits of adsorbate mixture of E1, E2, EE2,
630 and E3 EHs on the adsorbent nanofibers using several model plots. In Fig. 5a, the plotting *In* (q_e-
631 q_t) vs. t for E3 hormone shows good compliance with the pseudo-first-order equation. The data
632 points are shown together with the generated lines of best fits. The agreement between the data
633 set is reflected by the high regression coefficient (0.962) for E3, and the equilibrium adsorption
634 capacity calculated for E3 (0.368) is extremely close to the experimental value (0.369), which
635 indicates that predicted adsorption capacity by this model is almost the same as the actual value.
636 The rate constant k_1 is much more similar and in the range for all EHs. However, this model
637 appears less accurate for E2, EE2, and E1 for describing the initial stage ($t \leq 30$ min). The
638 theoretical expected yield of 0.350, 0.444, and 0.306 seems unsatisfactory and far less than the
639 actual 0.532, 0.687, and 0.551 for E2, EE2, and E1.
640
641 The lines plotted in Fig. 5b of t/q_t vs. t must be linear to estimate q_e and k_2 from the slope and y-
642 intercept, respectively. The results indicated that the interaction of E2, EE2, and E1 with the
643 material followed a line of best fit, completely matching the data set points. The regression
644 coefficients are 0.99, and the calculated adsorption capacities of E2, EE2, and E1 are 0.544,
645 0.711, and 0.549 compared to the experimental values 0.532, 0.687, and 0.551, respectively. The
646 slight difference indicates that the active sites were not homogenous on the surface because the
647 adsorption rate is determined by the hormone concentration and the number of active sites
648 available on the material (Vazquez-Velez et al. 2020). These findings confirm the suitability of
649 this model for describing E1, E2, and EE2 adsorption on WCENFs. Similar results were
650 observed when comparing the results described in the literature for MWCNTs by Al-Khateeb *et*
651 *al.* (Al-Khateeb et al. 2014a). Whereas E3 is showing an overall non-linear trend; instead, two
652 linear portions can be seen. One for the first 60 min and the second for the time interval after 100
653 min. The plot in Fig. 5b was used to determine the rate constant (k_2) and the calculated
654 equilibrium adsorption capacity (q_e) expressed in Eq. (8) to obtain the regression coefficient (R^2)
655 shown below in Table 5.
656
657 Regarding Fig. 5c of q_t vs. $t^{0.5}$, the graph for E3 is a linear plot with a comparatively high
658 regression coefficient, but the plot does not passes through the origin. This specifies that the
659 intraparticle diffusion is not entirely the rate-limiting step, which is likely to happen in the

adsorption of the other three EHs as well, as shown in Fig. 5c. The plausible reason for EH could be that they do not converge properly and the overall best fits do not pass through the origin; this could be due to a surface effect that may have dominantly controlled the sorption process after an hour of time interval and be considered a diffusion-controlled or boundary layer diffusion effect. Furthermore, two linear trends can be seen clearly. In the first 60 min, a sharper and steeper slope trend of a line is observed, which could pass through the origin, and it means that intraparticle diffusion is the rate-limiting step in this region. While in the second region, the diffusion slows down, shown by a gentle slope because the lesser remaining concentration of EHs is left in the solution. Thus, for E2, EE2, and E1, intra-particle diffusion can be part of the mechanism, but it can not be a total rate-determining step (Al-Khateeb et al. 2014a).

The plot in Fig. 5d of q_t vs. *In t* shows that EE2 has the highest regression coefficient (0.999), which explains that chemisorption is the most prominent mechanism for the adsorption of EE2 on WCENFs. This is also proven when EE2 had the most rapid adsorption (see Fig. 4a) and the highest equilibrium capacity of 0.687 mg/g compared to the other EHs.

In the case of Fig. 5e of *In* q_t vs. *In t*, a mismatch is seen for E3, while a linear relationship is seen for E1, E2, and EE2 but not for overall adsorption time. The regression coefficients were not satisfactory in most of the cases. This indicates that the fractional power model is not appropriate for EH. The calculated parameters using Eq. (8), (9), (10), (11), and (12) are shown in Table 5.

Table 5

The kinetic models parameters with each EH using WCENFs

Models	Hormones			
Parameters	Estrone (E1)	β-Estradiol (E2)	17α-Ethinylestradiol (EE2)	Estriol (E3)
Experimental q_e (mg/g)	0.551	0.532	0.687	0.369
Pseudo First Order model				
k_1 (min^{-1})	0.002	0.003	0.003	0.002

q_e, cal (mg/g)	0.306	0.350	0.444	0.368
R^2	0.951	0.958	0.977	0.962
Pseudo Second Order model				
k_2 (g/mg min)	0.055	0.045	0.041	0.012
q_e, cal (mg/g)	0.549	0.544	0.711	0.464
R^2	0.991	0.988	0.995	0.966
Intraparticle diffusion model				
k (mg/g $h^{1/2}$)	1.006	1.022	1.386	1.017
I (mg/g)	0.181	0.159	0.210	-0.017
R^2	0.931	0.975	0.926	0.996
Elovich Model				
α (g/mg min)	14.964	12.962	7.414	1.636
β (mg/g min)	0.081	0.080	0.112	0.077
R^2	0.994	0.979	0.999	0.930
Fractional power model				
A	0.113	0.108	0.123	0.007
B	0.255	0.255	0.286	0.663
Ab	0.368	0.362	0.409	0.669
R^2	0.973	0.994	0.967	0.969

3.4. Adsorption mechanism

The four possible adsorption mechanisms between EHs and the WCENFs could be (1) size-exclusion; (2) physical adsorption of estrogens on the external surface and inside layers of nanofibers due to their porous structures; (3) charge interactions between EHs and WCENFs; (4) Hydrogen bonding of EHs' molecules onto nanofibers by reaction with the functional groups present on the surface of nanofibers. Size exclusion is unexpected in this system because the reported molecular size of estrogens by Han *et al*. is quite small (approximately 0.8 nm for E1 and 0.796 nm for E2) than the pore sizes of the WCENFs (1.4 µm) and GMF filter (0.45 µm) used. Otherwise, the removal efficiency would have been 100%. A smaller fiber diameter in WCENFs (196 ± 65 nm) leads to a larger surface area (18.05 m^2/g) that provided sufficient active sites for adsorption of EHs on the nanofibers, as shown in Table 2. The electrostatic

charge might also influence adsorption, as Porter and Porter already reported adsorption behavior on microfilters in the presence of cations (Porter and Porter 1995). The deprotonation of E1, E2, EE2, and E3 is governed by the hydroxyl group's dissociation attached to the benzene ring. The acid dissociation constants for E1, E2, EE2 and E3 are 10.34, 10.46, 10.4 and 10.38, respectively (Auriol et al. 2006; Behera et al. 2011). All of them have slightly weaker acidity than phenol (pK_a = 10). As a result of the high value of pKa, most of the molecules for all these estrogens are undissociated; thus, they stay neutral in the solution mixture (Nghiem and Schäfer 2002; Bayode et al. 2021a). As a result, it is unlikely that the influence of charge interaction can be the main factor for the significant adsorption of these EHs on the nanofibers (Han et al. 2010a).

The high and rapid adsorption of the EHs on the WCENFs is particularly interesting. The size of molecules is far tiny compared to the porosity of this nanostructure. Therefore, the pore size has negligible dependence on adsorption. Apart from the physical adsorption, which gradually reaches equilibrium, the only rational explanation is the strong interaction of these EHs with the nanofibers due to the bonding. Hydrogen bonds are more robust than the Van der Waals forces involved in the physical adsorption. Fig. 6 below shows the chemical interactions of each EH with the WCENFs molecule.

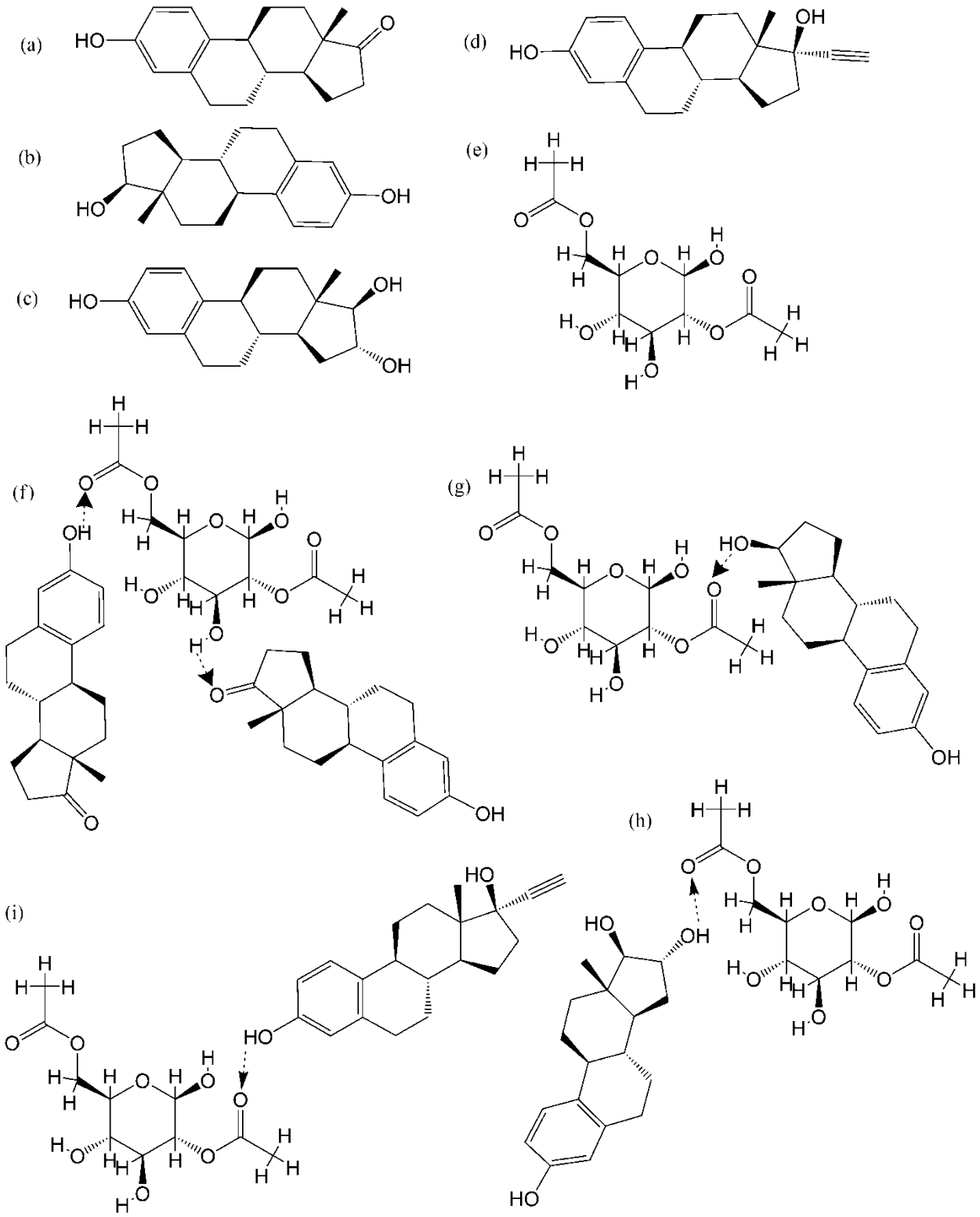

712

713 **Fig. 6** Displayed structures of (a) E1, (b) E2, (c) E3, (d) EE2, (e) WCENFs molecule and

714 hydrogen bonding between WCENFs molecule with EHs (f) E1, (g) E2, (h) E3, and (i) EE2

The EH molecules (E1, E2, EE2, E3) in this study contain a hydroxyl group (-OH) acting as a proton donor for hydrogen bonding. Due to the presence of both nucleophilic carbonyl group (-C=O) and hydroxyl group in E1, this proton can act as both donor or acceptor in the hydrogen bonding because CA also contains both C=O and O-H groups. Han *et al*. have described and explained similar hydrogen bonding of E1 with nylon 6,6 membrane in their investigation (Han et al. 2010a, 2012). Nylon 6,6 and cellulose acetate have a common C=O functional group involved in the hydrogen bonding with the estrogens during the adsorption process. Therefore, the functional groups (C=O), (C-O-C), and (C-O-H) present in WCENFs are involved in hydrogen bonding due to lone pair electrons present on oxygen atoms with (C=O) and (O-H) groups present in E1, whereas only (O-H) group of the other three EHs (E2, EE2, and E3) is involved in chemisorption as shown in Fig. 6 and presented in FTIR analysis in Fig. 7. These hydrogen bonding interactions would dictate the EHs' adsorption on WCENFs, explaining the fast adsorption process for EHs in the initial stage of the experiment. FTIR analysis is a sensitive technique used in the study to characterize the hydrogen bonds on WCENFs, as shown below.

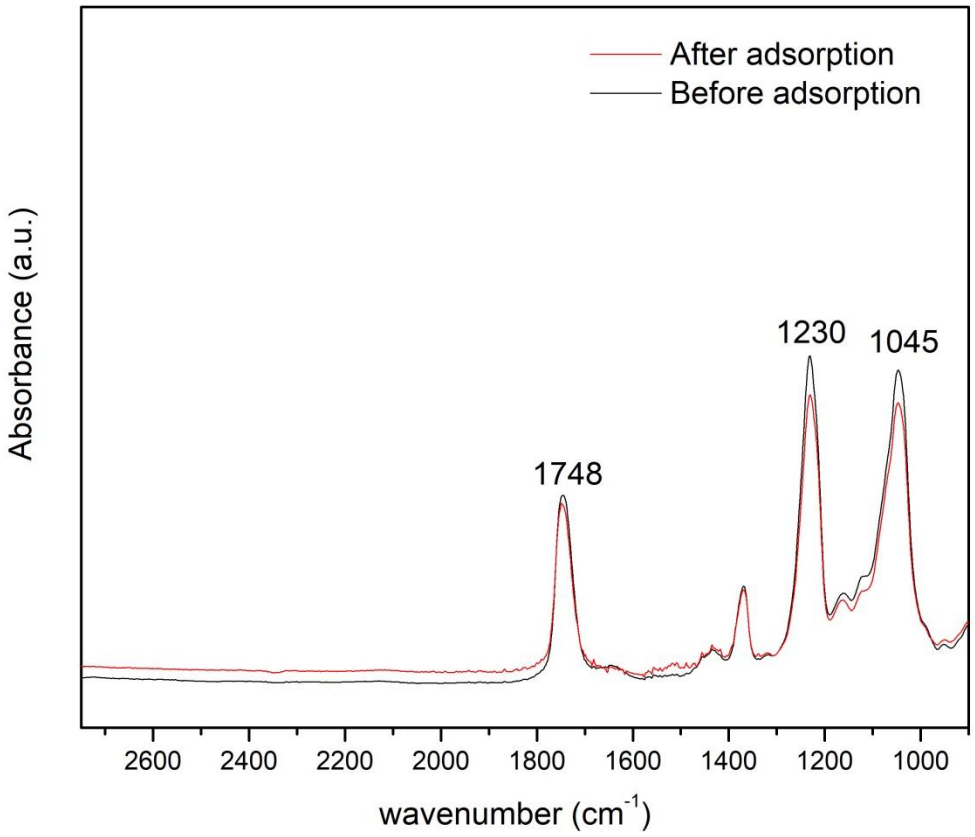

Fig. 7 FTIR spectra of WCENFs before and after batch adsorption (0.8 mg/L mixture of E1, E2, EE2. and E3, 100 mL)

The superimposed FTIR spectra of WCENFs before and after the adsorption study are presented in Fig. 7. It is noteworthy to see the difference in the peak's relative intensities at 1748 cm^{-1}, 1230 cm^{-1}, and 1045 cm^{-1} corresponding to C=O stretching, C-O-C anti-symmetric stretching, and C-O bonds, respectively (Nasir et al. 2017). Their intensities significantly decrease after the adsorption study due to the developed inter-molecular hydrogen bonding interactions. In contrast, no change is noticed in the C-CH_3 (1369 cm^{-1}) band because it can not undergo hydrogen bonding. This assures the existence of the chemisorption at 1748 cm^{-1}, 1230 cm^{-1}, and 1045 cm^{-1} of all these EHs on nanofibers' surface. In addition, The variation in the peak intensity depends on the number of active available functional groups present in the system and their competing behavior for the available sites because we should not forget that these free groups on nanofibers could also react with other proton donor species present in the system, for instance, water that could even form new hydrogen bonds (Han et al. 2012). Hence, the results supporting the previous literature suggest that EHs (E1, E2, EE2, E3) could form hydrogen bonding with oxygen-containing groups on WCENFs (Han et al. 2010b; Bayode et al. 2021b; Filep et al. 2021).

3.5. Determination of recovery and reusability

The adsorption and desorption process was repeated for four consecutive cycles, and considering the efficiency of WCENFs below 10% during the 4th cycle, it was not further reused. The adsorption study of each cycle is reported in Fig. 8.

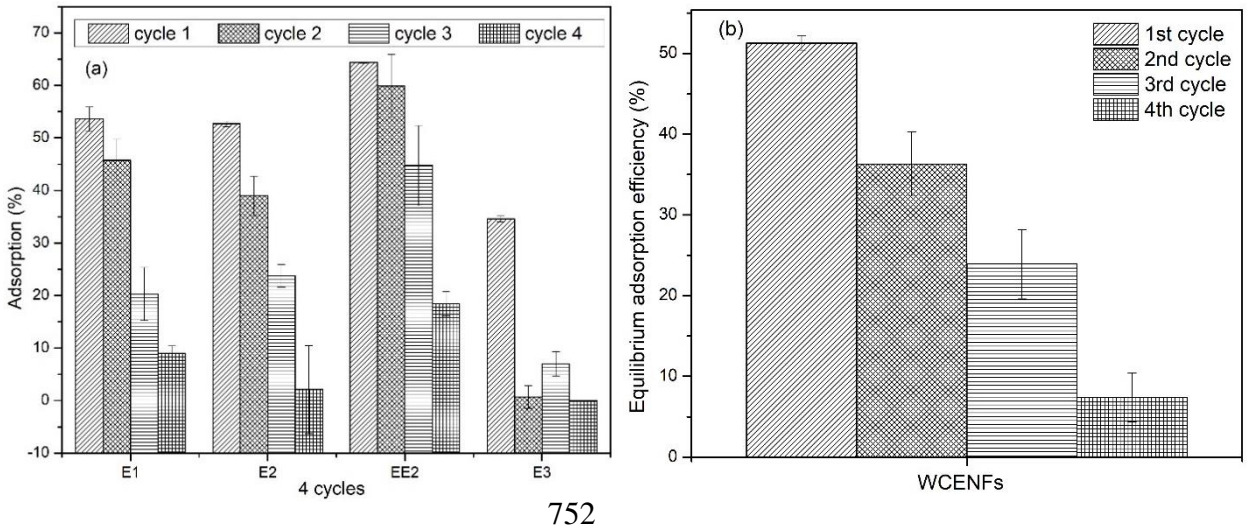

Fig. 8 (a) Adsorption cycles of each EH (E1, E2, EE2, E3) with an initial concentration of 0.2 mg/L in a combined solution of 0.8 mg/L on WCENFs (20 mg), (b) Cumulative efficiency of all EHs adsorption on WCENFs during four cycles

Fig. 8a represents the percentage removal of each EH concurrently on WCENFs during four consecutive adsorption cycles. As can be seen, the trend is decreasing after every successive cycle for all EHs except for E3, where the adsorption percentage remains below 10% after the first cycle due to fewer available active sites for adsorption and intense competition among the functional groups of EHs. The highest removal efficiencies are observed for EE2 (~64.3%), and least for E3 (~34.6%), and the trend is similar in each adsorption cycle. The gradual decrease in adsorption after each cycle is because of mass loss during the desorption process, leading to a reduction of the active adsorptive sites and, thus, a drop in the surface area due to the increase in the fiber diameter (see Fig. 9).

Fig. 8b above illustrates the equilibrium adsorption efficiency of WCENFs for cumulative EH removal during four adsorption cycles. As can be seen, the highest reduction of EHs in the first cycle is 51.3%, and the trend follows a gradual decrease which ends at 7.4% in the fourth adsorption cycle. Furthermore, it should also be noted that due to the continuous treatment with ethanol during desorption, it was evident that the nanofibers became stiff and shrank due to mass loss after the last cycle. Therefore, nanofibers were compact and tightly folded, providing less surface area for EH entrapment during the previous cycle. Thus, providing lesser removal efficiency. The presented comparison was made as a modeling study for the reusability of nanostructure from WCENFs for sorption. In industrial applications, some other solvents have to be tested. According to this model study, the more requested properties of a suitable solvent must be a very high solubility of EH with no solubility of the polymer.

With the repeated desorption cycles of EHs from nanofibers using ethanol, there was a significant change in the fiber morphology attributed to the contact of nanofibers with ethanol. However, nanofibers were unlikely to dissolve in ethanol, and their porous structure allowed complete penetration of ethanol molecules. Therefore, after several cycles and contact time, it has led to collapse and swelling of the nanofibers structure and the effectiveness of the

adsorption process (Schäfer et al. 2018). It is evident in the SEM image of the nanofiber structure after the complete adsorption study, as shown.

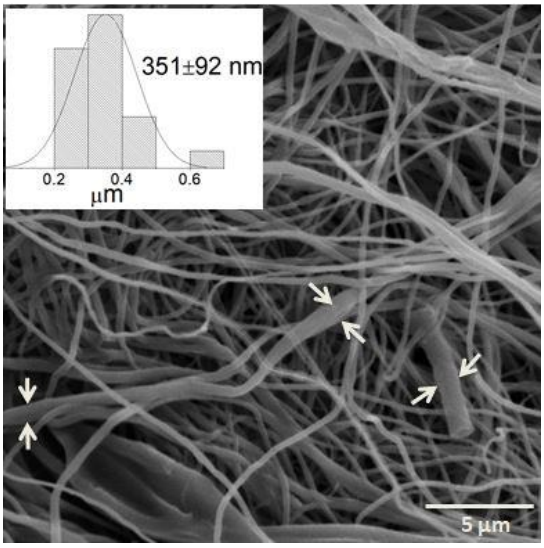

Fig. 9 SEM Image of WCENFs and their fiber diameter distribution after four adsorption-desorption cycles

Fig. 9 shows the nanofiber's surface morphology after four adsorption-desorption cycles. As can be seen, the nanofiber's diameter increased from 196-351 nm, with the high swelling experienced on several nanofibers as shown above (white arrows).

3.6. EH adsorption on WCENFs fabricated membrane filter and commercial application

The adsorption equilibrium of EH solution was observed in these filters, and a characteristic value of volume to reach equilibrium (V_{eq}) was noted. This concept of determining V_{eq} is used to conveniently and approximately mitigate the effect of these hormones simultaneously on WCENFs. V_{eq} is defined as the minimum volume of feed solution that passes through the filter that can withstand to achieve adsorption equilibrium for this set of EHs. Suppose the value of V_{eq} is significantly considerable. In that case, this method can be used for the instant removal of EHs from wastewater. Fig. 10 below shows the comparative results of E1, E2, EE2, and E3 adsorption in the WCENFs filter, where the residual concentration of the mixed EH solution permeates normalized (expressed in percentage values) against the initial concentration of each hormone in the feed versus the accumulated feed solution. It must be noted that these results are compared with the commercial CA filter reported by Han *et al*. for E1 adsorption.

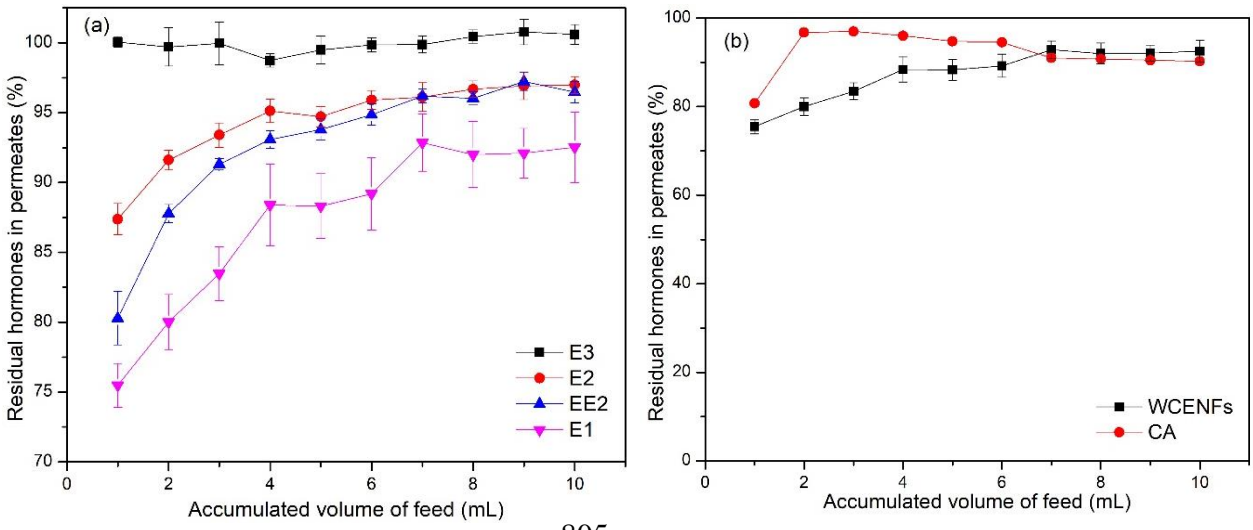

805

806 **Fig. 10** (a) Concurrent adsorption of EHs (E1, E2, EE2, and E3) on 1.4 µm WCENFs filter using
807 0.8 mg/L EH aqueous solution as feed containing 0.2 mg/L of each hormone and (b) 1.4 µm
808 WCENFs filter adsorption comparison with 0.45 µm commercial CA filter for E1 (Han et al.
809 2010b)

810 Fig. 10a shows simultaneous adsorption of all EHs on the WCENFs filter. It can be seen that the
811 highest adsorption is experienced for E1 and the lowest for E3 until equilibrium was achieved at
812 7 mL. It can be seen that maximum adsorption for E1, E2, EE2, and E3 were found to be 24.5%,
813 12.6%, 19.7%, and 0.5%, respectively. A gradual decrease in adsorption was seen for WCENFs
814 in a continuous filtration process, which suggests the physical adsorption of EH on WCENFs.
815
816 Fig. 10b compares the filter results produced from WCENFs with the commercial CA till the end
817 filter capacity of 10 mL was reached. As can be seen, the total E1 adsorption of 18.6% was seen
818 for commercial CA with the initial solution concentration of 0.4 mg/L while 24.5% for WCENFs
819 with the initial concentration of 0.2 mg/L and 14.2% total adsorption for a combination of all
820 four EHs with solution concentration of 0.8 mg/L which is twice that of commercial CA. Then
821 after the 1st mL of permeate of commercial CA, a decrease in adsorption was observed
822 drastically during the next few permeates for commercial CA and then a slight increase in
823 adsorption until it gets stagnant, which could be due to experimental error or loss of some
824 already adsorbed E1 molecules. While, a gradual decrease in adsorption was seen for WCENFs
825 in a continuous filtration process, which suggests that physical adsorption could be the primary
826 cause of EH adsorption with any losses on WCENFs. The membrane's adsorption sites were
827 occupied by hormone molecules when more and more feed was passed, and eventually, an

828 equilibrium was established when the adsorption sites were saturated. The derived V_{eq} value was
829 7 mL for both WCENFs and commercial CA. After these volumes, no significant change was
830 observed. This suggests that the filter reached saturation with EH at 7 mL. Similar results were
831 reported in the literature for E1 adsorption reaching equilibrium at 8 mL for PP, 7 mL for PTFE,
832 and 6 mL for RC filters (Han et al. 2010b).
833
834 The WCENFs filter in the current study has a high retention volume for these EHs with twice the
835 initial concentration of EH solution compared to the commercial GMF, RC, PTFE, CA, and PP
836 filters reported by Han *et al*. Therefore, WCENFs can be used within this capacity for instant and
837 concurrent removal of these EH solutes from wastewater. It can be a cheap and viable method by
838 using waste CBs to make a WCENFs filter for replacing the commercially available filter for
839 water treatment. The WCENFs filter can be an excellent substitute for the already available
840 commercial filters.
841
842 **Conclusions**
843 This study focused on concurrent removal of four EHs (E1, E2, EE2, E3) to replicate real-time
844 waste streams using WCENFs, recycling, and green approach. A one-step detection and
845 concomitant quantification method based on HPLC was devised for these EHs. It is noteworthy
846 to mention that the WCENFs membrane was capable of successfully removing all of these EHs.
847 The chemical composition of polymer, functional groups present, and structure of WCENFs
848 played an essential role in the rapid adsorption process, which is elaborated in the adsorption
849 mechanism. The highest percentage removal efficiencies were 64.3%, 53.6%, 52.7%, and 34.6%
850 for EE2, E1, E2, and E3, respectively. The total adsorption capacity obtained was 2.14 mg/g and
851 reported individual adsorption capacities of E1, E2, EE2, and E3 were found to be 0.551, 0.532,
852 0.687, and 0.369 mg/g, respectively. Based on the kinetic modeling results, the pseudo-first-
853 order suits E3 and the pseudo-second-order model is suitable for E1, E2, and EE2. Therefore,
854 both models are considered most appropriate due to their high regression coefficients than the
855 other kinetic models. Desorption studies for the recovery of EHs and reuse of sorption
856 nanostructure were conducted and validated for four cycles. To summarize, the fabricated
857 WCENFs membrane filter successfully responded to retention time for these EHs compared to
858 commercial CA filters. It also implies that recycled WCENFs can be considered a promising

adsorbent for rapidly remediation of wastewater streams and possibly replacing the commercially available CA syringe filters.

CrediT authorship contribution statement

Muhammad Yasir: Conceptualization, Methodology, Investigation, Formal analysis, Data curation, Writing- original draft, Writing- Review & editing.
Tomáš Šopík: Methodology, Formal analysis, Data curation.
Rahul Patwa: Formal analysis, Data curation, Review & editing.
Dušan Kimmer: Conceptualization, Supervision, Review & editing.
Vladimír Sedlařík: Conceptualization, Supervision, Project administration, Funding acquisition, Review & editing.

Declaration of competing interest

The authors declare that they have no known competing financial interests or personal relationships that could influence the work reported in this article.

Acknowledgments

The authors gratefully acknowledge the financial support by the Ministry of Education, Youth, and Sports of the Czech Republic (grant no. RP/CPS/2020/002), the Internal Grant Agency of TBU in Zlin (grant no. IGA/CPS/2021/002). We would also like to acknowledge the Centre of Polymer Systems (CPS) situated at Tomas Bata University in Zlin, Czech Republic, to use the available research facilities to conduct this research work. Furthermore, the authors very much appreciate the assistance in laboratory equipment by Dr. Lenka Lovecka in CPS.

REFERENCES

Abdel-Gawad SA, Abdel-Aziz HM (2019) Removal of ethinylestradiol by adsorption process from aqueous solutions using entrapped activated carbon in alginate biopolymer: isotherm and statistical studies. Appl Water Sci 9:1–8. https://doi.org/10.1007/s13201-019-0951-7

Adeel M, Song X, Wang Y, et al (2017) Environmental impact of estrogens on human, animal and plant life: A critical review. Environ. Int. 99:107–119

Al-Khateeb LA, Obaid AY, Asiri NA, Abdel Salam M (2014a) Adsorption behavior of

estrogenic compounds on carbon nanotubes from aqueous solutions: Kinetic and thermodynamic studies. J Ind Eng Chem 20:916–924. https://doi.org/10.1016/j.jiec.2013.06.023

Al-Khateeb LA, Obaid AY, Asiri NA, Abdel Salam M (2014b) Adsorption behavior of estrogenic compounds on carbon nanotubes from aqueous solutions: Kinetic and thermodynamic studies. J Ind Eng Chem 20:916–924. https://doi.org/10.1016/j.jiec.2013.06.023

Alhokbany NS, Naushad M, Kumar V, et al (2020) Self-nitrogen doped carbons aerogel derived from waste cigarette butts (cellulose acetate) for the adsorption of BPA: Kinetics and adsorption mechanisms. J King Saud Univ - Sci 32:3351–3358. https://doi.org/10.1016/j.jksus.2020.09.021

Ali H, Guler AC, Masar M, et al (2021) Solid-state synthesis of direct z-scheme cu2o/wo3 nanocomposites with enhanced visible-light photocatalytic performance. Catalysts 11:1–26. https://doi.org/10.3390/catal11020293

Aris AZ, Shamsuddin AS, Praveena SM (2014) Occurrence of 17α-ethynylestradiol (EE2) in the environment and effect on exposed biota: A review. Environ. Int. 69:104–119

Arroyo FD, Castro-Guerrero CF, León-Silva U (2020) Thin films of cellulose acetate nanofibers from cigarette butt waste. Prog Rubber, Plast Recycl Technol 36:3–17. https://doi.org/10.1177/1477760619895024

Augusto F, Hantao LW, Mogollón NGS, Braga SCGN (2013) New materials and trends in sorbents for solid-phase extraction. TrAC - Trends Anal Chem 43:14–23. https://doi.org/10.1016/j.trac.2012.08.012

Auriol M, Filali-Meknassi Y, Adams CD, Tyagi RD (2006) Natural and synthetic hormone removal using the horseradish peroxidase enzyme: Temperature and pH effects. Water Res 40:2847–2856. https://doi.org/10.1016/j.watres.2006.05.032

Bayode AA, dos Santos DM, Omorogie MO, et al (2021a) Carbon-mediated visible-light clay-Fe2O3–graphene oxide catalytic nanocomposites for the removal of steroid estrogens from water. J Water Process Eng 40:101865. https://doi.org/10.1016/j.jwpe.2020.101865

Bayode AA, dos Santos DM, Omorogie MO, et al (2021b) Carbon-mediated visible-light clay-Fe2O3–graphene oxide catalytic nanocomposites for the removal of steroid estrogens from water. J Water Process Eng 40:101865. https://doi.org/10.1016/j.jwpe.2020.101865

Behera SK, Kim HW, Oh JE, Park HS (2011) Occurrence and removal of antibiotics, hormones and several other pharmaceuticals in wastewater treatment plants of the largest industrial city of Korea. Sci Total Environ 409:4351–4360. https://doi.org/10.1016/j.scitotenv.2011.07.015

Benavente MJ, Caballero MJA, Silvero G, et al (2019) Cellulose Acetate Recovery from Cigarette Butts. Proceedings 2:1447. https://doi.org/10.3390/proceedings2201447

Bhardwaj N, Kundu SC (2010) Electrospinning: A fascinating fiber fabrication technique. Biotechnol. Adv. 28:325–347

Bilge S, Bakirhan NK, Osman Donar Y, et al (2019) Turning toxic cigarette butt waste into the sensor material for the sensitive determination of antihypertensive drug trandolapril from its dosage form and biological samples. Sensors Actuators, B Chem 296:. https://doi.org/10.1016/j.snb.2019.126626

Braga O, Smythe GA, Schäfer AI, Feitz AJ (2005) Fate of steroid estrogens in Australian inland and coastal wastewater treatment plants. Environ Sci Technol 39:3351–3358. https://doi.org/10.1021/es0501767

Cartinella JL, Cath TY, Flynn MT, et al (2006) Removal of natural steroid hormones from wastewater using membrane contactor processes. Environ Sci Technol 40:7381–7386. https://doi.org/10.1021/es060550i

Celebioglu A, Demirci S, Uyar T (2014) Cyclodextrin-grafted electrospun cellulose acetate nanofibers via “click” reaction for removal of phenanthrene. Appl Surf Sci 305:581–588. https://doi.org/10.1016/j.apsusc.2014.03.138

Chen Y, Zhang Y, Luo L, et al (2018) A novel templated synthesis of C/N-doped β-Bi2O3 nanosheets for synergistic rapid removal of 17α-ethynylestradiol by adsorption and photocatalytic degradation. Ceram Int 44:2178–2185. https://doi.org/10.1016/j.ceramint.2017.10.173

Chigome S, Darko G, Torto N (2011) Electrospun nanofibers as sorbent material for solid phase extraction. Analyst 136:2879–2889

Chigome S, Torto N (2011) A review of opportunities for electrospun nanofibers in analytical chemistry. Anal. Chim. Acta 706:25–36

Ersali S, Hadadi V, Moradi O, Fakhri A (2013) Pseudo-second-order kinetic equations for modeling adsorption systems for removal of ammonium ions using multi-walled carbon

nanotube. Fullerenes, Nanotub Carbon Nanostructures 150527104639002. https://doi.org/10.1080/1536383x.2013.787610

Esmaeeli F, Gorbanian SA, Moazezi N (2017) Removal of Estradiol Valerate and Progesterone using Powdered and Granular Activated Carbon from Aqueous Solutions. Int J Environ Res 11:695–705. https://doi.org/10.1007/s41742-017-0060-0

Filep T, Szabó L, Kondor AC, et al (2021) Evaluation of the effect of the intrinsic chemical properties of pharmaceutically active compounds (PhACs) on sorption behaviour in soils and goethite. Ecotoxicol Environ Saf 215:. https://doi.org/10.1016/j.ecoenv.2021.112120

Gopakumar DA, Pasquini D, Henrique MA, et al (2017) Meldrum's acid modified cellulose nanofiber-based polyvinylidene fluoride microfiltration membrane for dye water treatment and nanoparticle removal. ACS Sustain Chem Eng 5:2026–2033. https://doi.org/10.1021/acssuschemeng.6b02952

Günay A, Arslankaya E, Tosun I (2007) Lead removal from aqueous solution by natural and pretreated clinoptilolite: Adsorption equilibrium and kinetics. J Hazard Mater 146:362–371. https://doi.org/10.1016/j.jhazmat.2006.12.034

Gyllenhammar I, Glynn A, Jönsson BAG, et al (2017) Diverging temporal trends of human exposure to bisphenols and plastizisers, such as phthalates, caused by substitution of legacy EDCs? Environ Res 153:48–54. https://doi.org/10.1016/j.envres.2016.11.012

Han J, Qiu W, Cao Z, et al (2013) Adsorption of ethinylestradiol (EE2) on polyamide 612: Molecular modeling and effects of water chemistry. Water Res 47:2273–2284. https://doi.org/10.1016/j.watres.2013.01.046

Han J, Qiu W, Gao W (2010a) Adsorption of estrone in microfiltration membrane filters. Chem Eng J 165:819–826. https://doi.org/10.1016/j.cej.2010.10.024

Han J, Qiu W, Gao W (2010b) Adsorption of estrone in microfiltration membrane filters. Chem Eng J 165:819–826. https://doi.org/https://doi.org/10.1016/j.cej.2010.10.024

Han J, Qiu W, Hu J, Gao W (2012) Chemisorption of estrone in nylon microfiltration membranes: Adsorption mechanism and potential use for estrone removal from water. Water Res 46:873–881. https://doi.org/10.1016/j.watres.2011.11.066

He J, Zhou Q, Guo J, Fang F (2018) Characterization of potassium hydroxide modified anthracite particles and enhanced removal of 17α-ethinylestradiol and bisphenol A. Environ Sci Pollut Res 25:22224–22235. https://doi.org/10.1007/s11356-018-2287-5

983 Hemamalini T, Karunakaran SA, Siva Elango MK, et al (2019) Regeneration of cellulose acetate
984 nanofibrous mat from discarded cigarette butts. Indian J Fibre Text Res 44:248–252
985 Ho YS, McKay G (2002) Application of kinetic models to the sorption of copper (II) on to peat.
986 Adsorpt Sci Technol 20:797–815. https://doi.org/10.1260/026361702321104282
987 Hristovski KD, Nguyen H, Westerhoff PK (2009) Removal of arsenate and 17α-ethinyl estradiol
988 (EE2) by iron (hydr)oxide modified activated carbon fibers. J Environ Sci Heal - Part A
989 Toxic/Hazardous Subst Environ Eng 44:354–361.
990 https://doi.org/10.1080/10934520802659695
991 Jin X, Hu JY, Tint ML, et al (2007) Estrogenic compounds removal by fullerene-containing
992 membranes. Desalination 214:83–90. https://doi.org/10.1016/j.desal.2006.10.019
993 Johnson AC, Aerni HR, Gerritsen A, et al (2005) Comparing steroid estrogen, and nonylphenol
994 content across a range of European sewage plants with different treatment and management
995 practices. Water Res 39:47–58. https://doi.org/10.1016/j.watres.2004.07.025
996 Kimmer D, Vincent I, Fenyk J, et al (2011) Morphology of nano and micro fiber structures in
997 ultrafine particles filtration. In: AIP Conference Proceedings. pp 295–311
998 Kimmer D, Vincent I, Lovecka L, et al (2017) Some aspects of applying nanostructured
999 materials in air filtration, water filtration and electrical engineering. In: AIP Conference
1000 Proceedings
1001 Kiran Kumar A, Venkata Mohan S (2012) Removal of natural and synthetic endocrine disrupting
1002 estrogens by multi-walled carbon nanotubes (MWCNT) as adsorbent: Kinetic and
1003 mechanistic evaluation. Sep Purif Technol 87:22–30.
1004 https://doi.org/10.1016/j.seppur.2011.11.015
1005 Krupadam RJ, Sridevi P, Sakunthala S (2011) Removal of endocrine disrupting chemicals from
1006 contaminated industrial groundwater using chitin as a biosorbent. J Chem Technol
1007 Biotechnol 86:367–374. https://doi.org/10.1002/jctb.2525
1008 Kumar AK, Mohan SV (2011) Endocrine disruptive synthetic estrogen (17α-ethynylestradiol)
1009 removal from aqueous phase through batch and column sorption studies: Mechanistic and
1010 kinetic analysis. Desalination 276:66–74. https://doi.org/10.1016/j.desal.2011.03.022
1011 Kumar AK, Mohan SV, Sarma PN (2009) Sorptive removal of endocrine-disruptive compound
1012 (estriol, E3) from aqueous phase by batch and column studies: Kinetic and mechanistic
1013 evaluation. J Hazard Mater 164:820–828. https://doi.org/10.1016/j.jhazmat.2008.08.075

1014 Limpiyakorn T, Homklin S, Ong SK (2011) Fate of estrogens and estrogenic potentials in
1015 sewerage systems. Crit Rev Environ Sci Technol 41:1231–1270.
1016 https://doi.org/10.1080/10643380903488680
1017 Luo L, Yang Y, Xiao M, et al (2015) A novel biotemplated synthesis of TiO2/wood charcoal
1018 composites for synergistic removal of bisphenol A by adsorption and photocatalytic
1019 degradation. Chem Eng J 262:1275–1283. https://doi.org/10.1016/j.cej.2014.10.087
1020 Luo Y, Guo W, Ngo HH, et al (2014) A review on the occurrence of micropollutants in the
1021 aquatic environment and their fate and removal during wastewater treatment. Sci. Total
1022 Environ. 473–474:619–641
1023 Luo Z, Li H, Yang Y, et al (2017) Adsorption of 17α-ethinylestradiol from aqueous solution onto
1024 a reduced graphene oxide-magnetic composite. J Taiwan Inst Chem Eng 80:797–804.
1025 https://doi.org/10.1016/j.jtice.2017.09.028
1026 Ma H, Burger C, Hsiao BS, Chu B (2012) Nanofibrous microfiltration membrane based on
1027 cellulose nanowhiskers. Biomacromolecules 13:180–186.
1028 https://doi.org/10.1021/bm201421g
1029 McLachlan JA, Simpson E, Martin M (2006) Endocrine disrupters and female reproductive
1030 health. Best Pract. Res. Clin. Endocrinol. Metab. 20:63–75
1031 Mikaeili F, Gouma PI (2018) Super Water-Repellent Cellulose Acetate Mats. Sci Rep 8:1–8.
1032 https://doi.org/10.1038/s41598-018-30693-2
1033 Montalvão MF, Chagas TQ, da Silva Alvarez TG, et al (2019) How leachates from wasted
1034 cigarette butts influence aquatic life? A case study on freshwater mussel Anodontites
1035 trapesiali. Sci Total Environ 689:381–389. https://doi.org/10.1016/j.scitotenv.2019.06.385
1036 Montes-Grajales D, Olivero-Verbel J (2015) EDCs databank: 3D-structure database of endocrine
1037 disrupting chemicals. Toxicology 327:87–94. https://doi.org/10.1016/j.tox.2014.11.006
1038 Nasir M, Subhan A, Prihandoko B, Lestariningsih T (2017) Nanostructure and Property of
1039 Electrospun SiO2-Cellulose Acetate Nanofiber Composite by Electrospinning. Energy
1040 Procedia 107:227–231. https://doi.org/10.1016/j.egypro.2016.12.133
1041 Nghiem LD, Schäfer AI (2002) Adsorption and transport of trace contaminant estrone in NF/RO
1042 membranes. Environ Eng Sci 19:441–451. https://doi.org/10.1089/109287502320963427
1043 Niavarani Z, Breite D, Prager A, et al (2021) Estradiol removal by adsorptive coating of a
1044 microfiltration membrane. Membranes (Basel) 11:1–13.

https://doi.org/10.3390/membranes11020099
Onesios KM, Yu JT, Bouwer EJ (2009) Biodegradation and removal of pharmaceuticals and personal care products in treatment systems: A review. Biodegradation 20:441–466
Pan B, Lin D, Mashayekhi H, Xing B (2008) Adsorption and hysteresis of bisphenol A and 17α-ethinyl estradiol on carbon nanomaterials. Environ Sci Technol 42:5480–5485. https://doi.org/10.1021/es8001184
Patwa R, Saha N, Sáha P (2020) Magnetic hydrogel based shoe insoles for prevention of diabetic foot. J Magn Magn Mater 514:167153. https://doi.org/10.1016/j.jmmm.2020.167153
Pendergast MM, Hoek EMV (2011) A review of water treatment membrane nanotechnologies. Energy Environ. Sci. 4:1946–1971
Pham TT, Nguyen VA, Van der Bruggen B (2013) Pilot-Scale Evaluation of GAC Adsorption Using Low-Cost, High-Performance Materials for Removal of Pesticides and Organic Matter in Drinking Water Production. J Environ Eng 139:958–965. https://doi.org/10.1061/(asce)ee.1943-7870.0000704
Pinto AM, Moreira S, Gonçalves IC, et al (2013) Biocompatibility of poly(lactic acid) with incorporated graphene-based materials. Colloids Surfaces B Biointerfaces 104:229–238. https://doi.org/10.1016/j.colsurfb.2012.12.006
Porter JJ, Porter RS (1995) Filtration studies of selected anionic dyes using asymmetric titanium dioxide membranes on porous stainless-steel tubes. J Memb Sci 101:67–81. https://doi.org/10.1016/0376-7388(94)00278-7
Qi FF, Cao Y, Wang M, et al (2014) Nylon 6 electrospun nanofibers mat as effective sorbent for the removal of estrogens: Kinetic and thermodynamic studies. Nanoscale Res Lett 9:1–10. https://doi.org/10.1186/1556-276X-9-353
Rebischung F, Chabot L, Biaudet H, Pandard P (2018) Cigarette butts: A small but hazardous waste, according to European regulation. Waste Manag 82:9–14. https://doi.org/10.1016/j.wasman.2018.09.038
Sarmah AK, Northcott GL, Leusch FDL, Tremblay LA (2006) A survey of endocrine disrupting chemicals (EDCs) in municipal sewage and animal waste effluents in the Waikato region of New Zealand. Sci Total Environ 355:135–144. https://doi.org/10.1016/j.scitotenv.2005.02.027
Schäfer AI, Stelzl K, Faghih M, et al (2018) Poly(ether sulfone) Nanofibers Impregnated with β-

Cyclodextrin for Increased Micropollutant Removal from Water. ACS Sustain Chem Eng 6:2942–2953. https://doi.org/10.1021/acssuschemeng.7b02214

Semião AJC, Schäfer AI (2010) Xenobiotics Removal by Membrane Technology: An Overview. pp 307–338

Shannon MA, Bohn PW, Elimelech M, et al (2008) Science and technology for water purification in the coming decades. Nature 452:301–310

Shen F, Tian D, Yang G, et al (2020) Deacetylation Processing of Waste Cigarette Butts for High-Titer Bioethanol Production toward a Clean Recycling Process. ACS Sustain Chem Eng 8:11253–11262. https://doi.org/10.1021/acssuschemeng.0c03979

Siegenthaler PF, Bain P, Riva F, Fent K (2017) Effects of antiandrogenic progestins, chlormadinone and cyproterone acetate, and the estrogen 17α-ethinylestradiol (EE2), and their mixtures: Transactivation with human and rainbowfish hormone receptors and transcriptional effects in zebrafish (Danio reri. Aquat Toxicol 182:142–162. https://doi.org/10.1016/j.aquatox.2016.11.001

Solomon GM, Schettler T (2000) Environment and health: 6. Endocrine disruption and potential human health implications. Cmaj 163:1471–1476

Sood S, Shekhar S, Santosh W (2017) Dimorphic placental stress: A repercussion of interaction between endocrine disrupting chemicals (EDCs) and fetal sex. Med Hypotheses 99:73–75. https://doi.org/10.1016/j.mehy.2017.01.002

Szewczyk PK, Ura DP, Metwally S, et al (2018) Roughness and fiber fraction dominated wetting of electrospun fiber-based porous meshes. Polymers (Basel) 11:. https://doi.org/10.3390/polym11010034

Taha AA, Wu Y na, Wang H, Li F (2012) Preparation and application of functionalized cellulose acetate/silica composite nanofibrous membrane via electrospinning for Cr(VI) ion removal from aqueous solution. J Environ Manage 112:10–16. https://doi.org/10.1016/j.jenvman.2012.05.031

Tian Y, Wu M, Liu R, et al (2011) Electrospun membrane of cellulose acetate for heavy metal ion adsorption in water treatment. Carbohydr Polym 83:743–748. https://doi.org/10.1016/j.carbpol.2010.08.054

Tijani JO, Fatoba OO, Petrik LF (2013) A review of pharmaceuticals and endocrine-disrupting compounds: Sources, effects, removal, and detections. Water Air Soil Pollut 224:.

https://doi.org/10.1007/s11270-013-1770-3
Torkashvand J, Farzadkia M (2019) A systematic review on cigarette butt management as a hazardous waste and prevalent litter: control and recycling. Environ Sci Pollut Res. https://doi.org/10.1007/s11356-019-04250-x
Torkashvand J, Farzadkia M, Sobhi HR, Esrafili A (2020) Littered cigarette butt as a well-known hazardous waste: A comprehensive systematic review. J Hazard Mater 383:121242. https://doi.org/10.1016/j.jhazmat.2019.121242
Vazquez-Velez E, Lopez-Zarate L, Martinez-Valencia H (2020) Electrospinning of polyacrylonitrile nanofibers embedded with zerovalent iron and cerium oxide nanoparticles, as Cr(VI) adsorbents for water treatment. J Appl Polym Sci 137:1–10. https://doi.org/10.1002/app.48663
Vymazal J, Březinová T, Koželuh M (2015) Occurrence and removal of estrogens, progesterone and testosterone in three constructed wetlands treating municipal sewage in the Czech Republic. Sci Total Environ 536:625–631. https://doi.org/10.1016/j.scitotenv.2015.07.077
Wang J, Pan K, Giannelis EP, Cao B (2013) Polyacrylonitrile/polyaniline core/shell nanofiber mat for removal of hexavalent chromium from aqueous solution: Mechanism and applications. RSC Adv 3:8978–8987. https://doi.org/10.1039/c3ra40616d
Wang M, Qu F, Jia R, et al (2016) Preliminary study on the removal of steroidal estrogens using TiO2-doped PVDF ultrafiltration membranes. Water (Switzerland) 8:1–12. https://doi.org/10.3390/w8040134
Yang Z, Peng H, Wang W, Liu T (2010) Crystallization behavior of poly(ε-caprolactone)/layered double hydroxide nanocomposites. J Appl Polym Sci 116:2658–2667. https://doi.org/10.1002/app
YASIR M, ŠOPÍK T, KIMMER D, SEDLAŘÍK V (2020) Facile HPLC technique for simultaneous detection of estrogentic hormones in wastewater. NANOCON 2020 Conf Proeedings 2020:272–276. https://doi.org/10.37904/nanocon.2020.3710
Ye X, Shang S, Zhao Y, et al (2021) Ultra-efficient adsorption of copper ions in chitosan–montmorillonite composite aerogel at wastewater treatment. Cellulose 7:. https://doi.org/10.1007/s10570-021-03976-7
Yudanova TN, Filatov IY, Afanasov IM (2016) Production of ultrafine cellulose acetate fibers. Theor Found Chem Eng 50:508–512. https://doi.org/10.1134/S004057951604031X

Zhang Y, Zhou JL (2005) Removal of estrone and 17β-estradiol from water by adsorption. In: Water Research. pp 3991–4003

Zhao J, Lu Z, He X, et al (2017) One-Step Fabrication of Fe(OH)3@Cellulose Hollow Nanofibers with Superior Capability for Water Purification. ACS Appl Mater Interfaces 9:25339–25349. https://doi.org/10.1021/acsami.7b07038

Supplementary Files

This is a list of supplementary files associated with this preprint. Click to download.

- Graphicalabstract.pdf
- supportingdata.pdf